Contemporary Mathematics
https://ojs.wiserpub.com/index.php/CM/

Research Article

# On Artificial Neural Network to Analyze Discrete Fractional Order COVID-19 Mathematical Model

**Sajid Shah[1], Kamal Shah[2,3*],Thabet Abdeljawad[2], Eiman[3†]**

[1] EIAS Data Science and Blockchain Lab, College of Computer and Information Sciences (CCIS), Prince Sultan University, Riyadh, Saudi Arabia
[2] Department of Mathematics and Sciences, Prince Sultan University, Riyadh, 11586, Saudi Arabia
[3] Department of Mathematics, University of Malakand Chakdara Dir(L), Khyber Pakhtunkhwa, 18000, Pakistan
E-mail: kshah@psu.edu.sa; eiman@uom.edu.pk

**Received:** 29 January 2026; **Revised:** 26 February 2026; **Accepted:** 4 March 2026

**Abstract:** A discrete type model for addressing the recent COVID-19 disease with vaccination class is considered in this research work. In this work, we integrate the harmonic mean type incidence rate into a new fractional-order discrete-time Susceptible-Vaccinated-Infected-Recovered (SVIR) epidemic model. For the considered model Disease Free Equilibrium (DFE) and Endemic Equilibrium (EE) are deduced and the basic reproductive number is also computed. Sensitivity analysis based on direct method is analyzed. The qualitative analysis and numerical investigations for the mentioned model are studied to understand the dynamical behavior. Stability analysis is deduced by using Ulam-Hyers (U-H) criteria. Further, we also investigate the concerned model through the Artificial Neural Networks (ANNs) technique which has recently attracted very well. Additionally, the simulated outcomes and ANNs are compared, and several metrics such as regression coefficient, Mean Square Error (MSE), and Root Mean Square Error (RMSE) are recorded and displayed graphically. We use the Levenberg-Marquardt algorithm to analyze the required computational results. Matlab 2023 software is used for computational purposes.

***Keywords***: fractional difference operator, Artificial Neural Networks (ANNs), harmonic mean, computations, Levenberg-Marquardt algorithm

**MSC:** 92D30, 92D25, 26A33, 39A30

## Abbreviation

| | |
|---|---|
| SVIR | Susceptible-Vaccinated-Infected-Recovered |
| DFE | Disease Free Equilibrium |
| EE | Endemic Equilibrium |
| (U-H) | Ulam-Hyers |
| ANNs | Artificial Neural Networks |
| MSE | Mean Square Error |
| RMSE | Root Mean Square Error |


DOI: https://doi.org/10.37256/cm.7220269699

# 1. Introduction

Researchers are using numerous techniques to investigate infectious diseases from different perspectives. In the biological sciences, epidemiology is an important branch that looks at all the factors which affect the presence of illnesses and disorders. Researchers are becoming more interested in the topic of epidemiology due to the recent epidemics of several diseases, such as COVID-19, Severe Acute Respiratory Syndrome (SARS), Dengue, and Ebola. Therefore, formulations of mathematical models of such diseases and investigating their dynamical behaviors have significant applications [1]. Because, these models can help in controlling and preventing the disease in speeding in society [2]. Plenty of research papers have been published on the area of mathematical models of infectious diseases [3]. Discrete time models and continuous time models are the two primary groups into which researchers have divided these models. Here, we highlight some discrete type work as [4].

Researchers use mathematical models with differential equations for continuous time models, while in the case of discrete time model difference equations are used extensively [5]. Additionally, compared to continuous-time epidemic models, discrete-time models exhibit more complex dynamics [6]. Therefore, researchers have extensively used discrete type models to investigate various diseases [7]. Here, we mention that vaccination is also an important process for reducing and controlling the diseases in a society [8]. By using vaccine, we can reduce the susceptibility of infectious disease in our society [9]. Researchers have significantly studied the effectiveness of vaccination through mathematical models in the last few years. For instance, authors [10] have established a dynamical model with vaccination procedure. In the same way, the mathematical model with vaccination class was studied for COVID-19 by researchers [11]. The COVID-19 infectious disease which was identified in 2019 in China. The World Health Organization (WHO) classified the disease to be a worldwide pandemic after it later spread to every country in 2020. Still the disease is present in many countries of the world and daily many death occur continually [12]. But the rapid transmission rate has now been controlled due to vaccination now available in most of the countries [13]. The concerned disease was greatly investigated by using mathematical models [14]. Researchers have applied continuous and discrete time models for its study. Researchers [15] studied COVID-19 models using fractional calculus. Alkhazzan et al. [16] have investigated a novel Susceptible-Vaccinated-Infected-Recovered (SVIR) epidemic model with jumps for understanding the dynamics of the spread of dual diseases.

In recent decades, Fractional Calculus (FC) has gained popularity due to its excellent use in mathematical modeling of a wide range of real-world issues. due to the fact that the topic is currently a popular field of study. This is because it has important applications in a number of real-world issues. Fractional-order derivatives are somewhat more accurate than typical integer-order derivatives because they are a valuable tool for assessing the memory effect across all processing and material types [17]. Memory effects are the notion that all of a system's previous states connect to its current states in a fractional order. Many researchers have focused their attention on discrete fractional calculus over the past few years [18]. Interesting applications of aforesaid area can be read in various fields of science and engineering [19]. For instance, Wu et al. [20] proposed the first chaotic fractional logistic map. In the last few years, researchers have extensively worked on investigating discrete type model with fractional calculus tools [21].

Here, it should be kept in mind that fractional order derivative in the Caputo sense has been used very well in studying mathematical models of COVID-19 [22]. Different dynamical systems of the aforementioned disease have been analyzed by using fractional order derivatives. Khan et al. [23] have studied a model of climate change on coastal ecosystems by using fractional calculus. Djeddi et al. [24] have deduced existence theory and numerical analysis for fractional order continuous and discrete time models of COVID-19. Researchers have recently shown a great deal of interest in Artificial Intelligence (AI)-based techniques such as Deep Neural Networks (DNNs) and Artificial Neural Networks (ANNs). Here, we remark that Computer programs called ANNs are developed for biology process and then train to work like the human brain processes information. There are many ANNs tools available in which some of them are vary famous like Neural Networks (NNs) and ANNs tools. Recently, various kinds of research work has been conducted on using the aforesaid AI tools. Here, we mentioned the contribution of researchers [25] who have presented details information about the basic of AI tools. Researchers [26] have conducted research on auto-progressive training of NNs constitutive models with details. Authors [27] have used NNs to investigate the COVID-19 disease model in 2022. Authors [28] have used the ANNs to

investigate an epidemic model of infectious disease. Recently, Abdeljawad et al. [29] extended deep NNs analysis for psychological model using advanced analysis. But AI models based on ANNs and epidemic compartmental models based on differential equations are effective tools for investigating the spread of COVID-19. However, these tools also failed in the aforementioned areas for the major reasons. For example, in AI models, the biological pattern is not explained, whereas in compartmental models, parameter estimation is limited. However, the AI models are increasingly using as a powerful tools to analyze epidemic models. Here, we remark that compared to conventional bilinear or standard incidence rates models, the inclusion of a harmonic mean-type incidence rate in COVID-19 models offers a more accurate depiction of disease transmission, especially by more accurately describing behavioral shifts and saturated infection rates. The benefit of this modeling approach is that it helps analyze the stability of endemic and disease-free equilibria and is less vulnerable to dramatic, large-value swings in data. In addition, when we are predicting COVID-19 transmission rates in situations where data may be distorted by isolated outbreaks, the harmonic mean is more steady and reliable than arithmetic or geometric means since it assigns less weight to significant outliers. Further, compared to other types, the harmonic mean type offers a smoother, more precise fit to pandemic data, improving its forecasting ability for epidemiological trends. In recent times, intelligent neural network for modeling has been studied [30]. Authors [31] have studied cholera dynamics through neural networks.

Since, the ANNs and the discrete type fractional order models have not well studied for COVID-19. Two different discrete type mathematical models of COVID-19 were investigated in [32, 33] respectively. Therefore, we formulate a model with harmonic mean type incidence rate under discrete fractional calculus tools. We establish its existence theory, numerical analysis and basic quantities. Mathematically an artificial neural network defines a function of the form $\mathbf{F}u = v$, $u \in R^m$, $v \in R^n$, where $m$, $n$ stand for input and output dimensions. An input $u \in R^m$ is feed to artificial neural network which produces output $v \in R^n$. The process is expressed mathematically as follows: $v = a_c(Wu + b)$, $W \in R^{m\times n}$, here $b \in R^n$ and $a_c$ is called activation function. The procedure is presented in Figure 1.

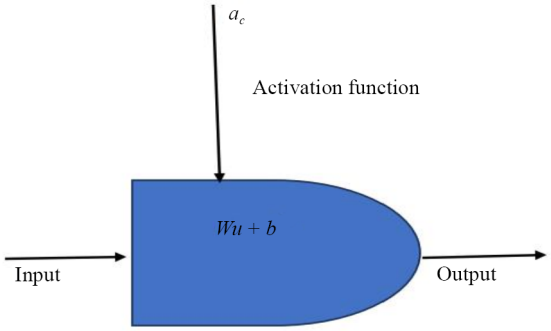


**Figure 1.** DDN process

We formulate a mathematical model with double harmonic mean type incidence rates involving vaccination class. We use the Cuputo Fractional Difference Operator (CFDO) to study the formulated model. Existence of solution and some stability results based on Ulam-Hyers (U-H) and basic results are established. Further, numerical illustrations for various compartments have been given. Finally, the simulated results are tested by using the ANNs techniques and various results including Mean Square Error (MSE), Root Mean Square Error (RMSE) and variance have been calculated and presented graphically for different compartments. The concerned ANNs have also some demerits which recently have been identified [34].

## 1.1 *Limitations*

Besides the mentioned advantages, some disadvantages also been identified which we list as:

• As discrete fractional calculus is being developed to examine memory-based systems on discrete time sets. Despite being helpful for modeling, it has also have some drawbacks and restrictions when compared to normal discrete calculus or continuous fractional calculus.

• Also variety of definitions of discrete fractional difference operators, some inconstancy occurred.

• For training such ANNs required powerful Graphics Processing Unit (GPU) and extensive time and hence cost expensive.

• As the model becomes large and complex, it will requires a lot of Random Access Memory (RAM) and storage space.

• It also considerable financial and environmental ramifications.

• Applications that demand accountability are severely limited by neural networks' inability to be interpreted.

• As the complexity goes up the model prediction given by ANNs is difficult to understand.

• The quantity and quality of training data is important in ANNs. Therefore, models with poor quality produce predictions that are problematic and may be unrealistic.

• Still no perfect ANN yet has been designed to accurately predict due to the uncertainty in real data.

### 1.2 *Our main objectives are as follows*

• To formulate a fractional discrete Susceptible-Vaccinated-Infected-Recovered (SVIR) model with harmonic-mean incidence.

• To derive Disease Free Equilibrium (DFE)/Endemic Equilibrium (EE) and reproduction numbers by using next generation matrix method.

• To investigate sensitivity analysis by using direct method.

• To deduce the qualitative analysis by using fixed point theorems and stability due to U-H.

• To numerical interpret the results by using various fractional order values.

• To built detailed analysis based on using ANNs.

• To compare the results of ANNs and numerical analysis.

**Organization of paper:** We in section 1 give a detail introduction and limitations of the proposed study. Section 2 contains formulation of model. Section 3 contains preliminaries. Section 4 contains qualitative analysis. Section 5 contains numerical analysis. Section 6 is devoted to AI based ANNs results. Section 7 contains conclusion.

## 2. Formulation of model

Here, we formulate our model on the following hypothesis:

• Let the individuals enter to susceptible class S at rate $(1-\mu)\Lambda$. The notation $\delta$ stands for death rate and the rate at which individuals who are vaccinated from susceptible class is denoted by $\psi$. The ratio at which susceptible becomes infected is expressed as $\frac{2\beta SI}{S+I}$.

• The rate at which people are vaccinated be $\mu\Lambda$ and the rate at which individuals who from vaccinated class transferred to infected be $\frac{2\alpha VI}{V+I}$. Further, the natural death in vaccinated class is represented by $\delta$. It has been found that after vaccination, individual becomes susceptible it may catch an infection whose rate we denoted by $\varphi$.

• The infection rate be $\beta$, where the infected class is denoted by I. Further, let the recovery rate be $\rho$ and the re-infection rate is represented by $\gamma$. The natural death is $\delta$. Mortality rate due to infectious is represented by $\omega$.

• The rate at which people get rid of infection is $\rho$, and the natural death is denoted by $\delta$, while re-infection rate is represented by $\gamma$. Recovered individuals again become susceptible, let denote the rate by $\xi$.

On the basis of the given hypothesis, the model formulated in (1) is presented in Figure 2.

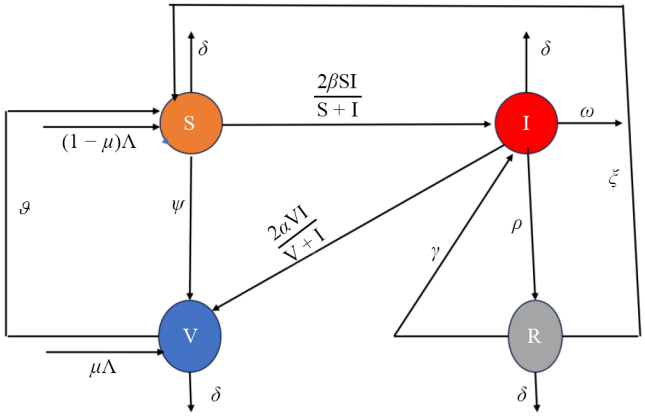


**Figure 2.** Flow chart of model (1)

Keeping these hypothesis in mind, we formulate the model in terms of differential equations as follows with $0 < \sigma \leq 1$:

$$\begin{aligned}
\dot{\mathrm{S}}(t) &= (1-\mu)\Lambda - \frac{2\beta \mathrm{SI}}{\mathrm{S}+\mathrm{I}} - (\delta+\psi)\mathrm{S} + \xi \mathrm{R} + \varphi \mathrm{V}, \ \ \mathrm{S}(0) > 0, \\
\dot{\mathrm{V}}(t) &= \mu\Lambda + \psi \mathrm{S} - \frac{2\alpha \mathrm{VI}}{\mathrm{V}+\mathrm{I}} - (\delta+\varphi)\mathrm{V}, \ \ \mathrm{V}(0) \geq 0, \\
\dot{\mathrm{I}}(t) &= \frac{2\beta \mathrm{SI}}{\mathrm{S}+\mathrm{I}} + \frac{2\alpha \mathrm{VI}}{\mathrm{V}+\mathrm{I}} - (\omega+\delta+\rho)\mathrm{I} + \gamma \mathrm{R}, \ \ \mathrm{I}(0) \geq 0, \\
\dot{\mathrm{R}}(t) &= \rho \mathrm{I} - (\delta+\gamma+\xi)\mathrm{R}, \ \ \mathrm{R}(0) \geq 0.
\end{aligned} \tag{1}$$

If the total population be $N$, then, we can easily show that

$$\dot{N}(t) \leq \Lambda - \delta N,$$

which on solving gives that

$$N(t) \to \frac{\Lambda}{\delta} + C_0 \Lambda \exp(-\delta t),$$

where $C_0$ is constant of integration. We see that at $t \to \infty$, one has the $N(t) \leq \frac{\Lambda}{\delta}$. Hence the feasible region for the bounded solution be defined as follows:

$$\Omega = \left\{ (\mathrm{S}, \mathrm{V}, \mathrm{I}, \mathrm{R}) : \ |(\mathrm{S}, \mathrm{V}, \mathrm{I}, \mathrm{R})| \leq \frac{\Lambda}{\delta} \right\}.$$

Moreover, if $(S(0), V(0), I(0), R(0)) > 0$, all compartments are positive because if we take from first equation of model (1)

$$\dot{S}(t) = (1-\mu)\Lambda - \frac{2\beta SI}{S+I} - (\delta+\psi)S + \xi R + \varphi V$$

$$> -(\delta+\psi)S,$$

which on solving gives that

$$S(t) > S(0)\exp(-((\delta+\psi)t) > 0,\ t > 0,$$

hence $S(t) > 0$, $t > 0$. We can prove for all other compartments in the same way. As discrete fractional calculus has also attracted attention very well. Therefore, researchable have taken keen interest in it to use in various real world problems. These operators produce output in the discrete form, which makes them ideal for studying real-world phenomena because real-world data is typically in this format [35]. Therefore, we will the mentioned difference operator with fractional order in our study. Moreover, theoretical and computational analysis will be established in details for the formulated model. For some details on applications of the aforesaid difference operator, we refer to [36, 37]. The modified form of our model (1) in fractional difference equations can be described as:

$$\begin{cases} {}^{C}\Delta^{\rho}S(t) = (1-\mu)\Lambda - \dfrac{2\beta S((t-1+\rho)I(t-1+\rho)}{S(t-1+\rho)+I(t-1+\rho)} - (\delta+\psi)S(t-1+\rho) + \xi R(t-1+\rho) \\ \qquad\qquad +\varphi V(t-1+\rho), \\ {}^{C}\Delta^{\rho}V(t) = \mu\Lambda + \psi S(t-1+\rho) - \dfrac{2\alpha V(t-1+\rho)I(t-1+\rho)}{V(t-1+\rho)+I(t-1+\rho)} - (\delta+\varphi)V(t-1+\rho), \\ {}^{C}\Delta^{\rho}I(t) = \dfrac{2\beta S(t-1+\rho)I(t-1+\rho)}{S(t-1+\rho)+I(t-1+\rho)} + \dfrac{2\alpha V(t-1+\rho)I(t-1+\rho)}{V(t-1+\rho)+I(t-1+\rho)} - (\omega+\delta+\rho)I(t-1+\rho) \\ \qquad\qquad +\gamma R(t-1+\rho), \\ {}^{C}\Delta^{\rho}R(t) = \rho I(t-1+\rho) - (\delta+\gamma+\xi)R(t-1+\rho). \end{cases} \tag{2}$$

Here, from additions of all equations of model (2), we get

$${}^{C}\Delta^{\rho}N(t) \leq \Lambda - \delta N(t). \tag{3}$$

Using discrete Laplace transform [38], we obtained from (3)

$$\mathscr{L}_b\{N\}(s) \leq \frac{s^{\rho-1}N(0)}{s^{\rho}-\delta(s+1)^{\rho}} + \frac{1}{(s+1)^{1-\rho}s^{\rho}-\delta}\mathscr{L}_b\{\Lambda\}(s).$$

Which gives the given result after evaluation

$$N(t) \leq N(0)E_{\rho,1}(\delta, t) + \frac{\Lambda}{\delta}\sum_{s=0}^{t-\rho} E_{\rho,\rho}(\delta, t-1-s).$$

Now, if $t \to \infty$, then we see that $E_{\rho,1}(\delta, t) \to 0$ and $E_{\rho,\rho}(\delta, t-1-s) \to 1$. Therefore, $N(t) \leq \frac{\Lambda}{\delta}$. Hence discrete population bound is obtained.

## 3. Preliminaries

Some fundamental results are given here.

**Definition 3.1** [37] Let $h$ be a function, then the $\phi$-CFDO is defined by

$$^{C}\Delta_b^{\rho}h(t) = \Delta_b^{-(n-\rho)}\Delta^n h(t) = \frac{1}{\Gamma(n-\rho)}\sum_{k=b}^{t-(n-\rho)}(t-k-1)^{n-\rho-1}\Delta^n h(k), \tag{4}$$

such that $t \in \mathbf{N}_{a+n-\rho}$, $n = \lceil \rho \rceil + 1$ for $\rho > 0$ and $\rho \notin \mathbf{N}$. Additionally we can express $(t-1-k)^{(n-\rho-1)}$, $\Delta^n h(k)$ represents $n$th integer order difference operator is defined as:

$$(t-k-1)^{(n-\rho-1)} = \frac{\Gamma(t-k)}{\Gamma(t-k-n+\rho+1)}, \tag{5}$$

and

$$^{C}\Delta^n h(t) = {}^{C}\Delta(^{C}\Delta^{n-1}h(t)) = \sum_{k=0}^{n}\binom{n}{k}(-1)^{n-k}h(t+k), \quad t \in \mathbf{N}_b. \tag{6}$$

If $n = 1$, we have $^{C}\Delta h(t) = h(t+\ell) - h(t)$. If $h(t) = t^3$, then for $n = 1, 2, 3$, we have

$$^{C}\Delta[t^3] = (t+\ell)^3 - t^3 = 3t^2\ell + 3t\ell^2 + \ell^3$$

$$^{C}\Delta^2[t^3] = 3\ell^2(2t+\ell) + 3\ell^3$$

$$^{C}\Delta^3[t^3] = 6\ell^3.$$

If $\ell = 1$, we get $\Delta^3[t^3] = 6$.

**Remark 3.2** For $n = 1$, the $\rho$-CFDO, we can write

$$ {}^{C}\Delta_b^{\rho} h(t) = \Delta_b^{-(1-\rho)} \Delta f(t) = \frac{1}{\Gamma(1-\rho)} \sum_{k=b}^{t-(1-\rho)} (t-k-1)^{-\rho} \Delta h(k), \tag{7} $$

such that $t \in \mathbf{N}_{b+1-\rho}$. Let $h(t) = (t-b)^{\mu}$, then

$$ {}^{C}\Delta^{\rho}[(t-b)^{\mu}] = \frac{\Gamma(\mu+1)}{\Gamma(\alpha-\mu+1)} (t-b)^{(\mu-\rho)}. $$

**Definition 3.3** [37] Taking $h$ on $\mathbf{N}_b$, where $h : \mathbf{N}_b \to \mathbb{R}$, then the $\rho$-the fractional sum of $h$ is written as:

$$ {}^{C}\Delta_b^{-\rho} h(t) = \sum_{k=b}^{t-\rho} \frac{(t-k-1)^{\rho-1} h(k)}{\Gamma(\rho)}, \tag{8} $$

such that time scale can be represented by $\rho > 0$, $t \in \mathbf{N}_{b+\rho} = \{b+\rho, b+\rho+1, \dots\}$ with $b \in \mathbb{R}$.

**Remark 3.4** [36] For $\rho > 0$ and $h$ over $\mathbf{N}_b$, we have

$$ {}^{C}\Delta^{-\rho} {}^{C}\Delta^{\rho} h(t) = h(t) - \sum_{k=0}^{n-1} \frac{(t-b)^{(k)}}{k!} \Delta^k h(b) $$

$$ = h(t) + c_0 + c_1(t-b) + \cdots + c_n (t-b)^{n-1}, $$

where $n$ is the smallest integer fulfills $n \geq \rho$, $c_i \in \mathbb{R}$, $i = 1, 2, \dots, n-1$.

**Remark 3.5** [36] Here for easiness, $\Gamma$ can be written as:

$$ \sum_{k=0}^{t-\rho} (t-k-1)^{(\rho-1)} = \frac{\Gamma(t+1)}{\rho\Gamma(t-\rho+1)}. \tag{9} $$

**Theorem 3.6** [39] The given fractional difference problem

$$ {}^{C}\Delta_b^{\rho} z(t) = h(\rho+t-1, z(\rho+t-1)), \ 0 < \rho \leq 1, $$

$$ \Delta^k z(t) = y_k, \ k = 0, 1, 2, ..., n-1, \ n = \lceil \rho \rceil + 1, \tag{10} $$

is given

$$z(t) = z_0(t) + \frac{1}{\Gamma(\rho)} \sum_{t=b+n-\rho}^{t-\rho} (t-s-1)^{\rho-1} h(\rho+s-1, z(\rho+s-1)),\ \ s \in \mathbf{N}_{b+\rho}, \tag{11}$$

where

$$z_0(t) = \sum_{k=0}^{n-1} \frac{(t-b)^k}{\Gamma(k+1)} \Delta^k z_k(b).$$

**Remark 3.7** Further, put $(t-1-s)^{(\rho-1)} = \dfrac{\Gamma((t-s)}{\Gamma(1-\rho+t-s)}$, and $b=0$, for (10), one may get

$$z(n) = z(0) + \frac{1}{\Gamma(\rho)} \sum_{i=0}^{n} \frac{\Gamma(n-i+\rho)}{\Gamma(n-i+1)} h(i-1, z(i-1)),\ \ s \in \mathbf{N}_{b+\rho}. \tag{12}$$

**Theorem 3.8** [40] Assume that $\mathscr{H} : \mathbb{C} \subset \mathbb{R}^n \to \mathbb{C} \subset \mathbb{R}^n$ is a continuous mapping with a nonempty, closed bounded and convex set, then $\mathscr{H}$ has at least one fixed point there.

## 4. Some qualitative results

Here, we deduce results related to boundedness, existence and positivity for the model (2). For the existence positivity we first write system (2) by using using $\nabla = t-1-s$ as follows:

$$\begin{aligned}
\mathrm{S}(t) &= \mathrm{S}(0) + \frac{1}{\Gamma(\rho)} \sum_{t=1-\rho}^{t-\rho} (\nabla)^{\rho-1} \Big[ (1-\mu)\Lambda - \frac{2\beta \mathrm{S}((t-1+\rho)\mathrm{I}(t-1+\rho)}{\mathrm{S}(t-1+\rho)+\mathrm{I}(t-1+\rho)} - (\delta+\psi)\mathrm{S}(t-1+\rho) \\
&\quad + \xi \mathrm{R}(t-1+\rho) + \varphi \mathrm{V}(t-1+\rho) \Big] \\
\mathrm{V}(t) &= \mathrm{V}(0) + \frac{1}{\Gamma(\rho)} \sum_{t=1-\rho}^{t-\rho} (\nabla)^{\rho-1} \Big[ \mu\Lambda + \psi \mathrm{S}(t-1+\rho) - \frac{2\alpha \mathrm{V}(t-1+\rho)\mathrm{I}(t-1+\rho)}{\mathrm{V}(t-1+\rho)+\mathrm{I}(t-1+\rho)} - (\delta+\varphi)\mathrm{V}(t-1+\rho) \Big] \\
\mathrm{I}(t) &= \mathrm{I}(0) + \frac{1}{\Gamma(\rho)} \sum_{t=1-\rho}^{t-\rho} (\nabla)^{\rho-1} \Big[ \mathrm{I}(0) + \frac{2\beta \mathrm{S}(t-1+\rho)\mathrm{I}(t-1+\rho)}{\mathrm{S}(t-1+\rho)+\mathrm{I}(t-1+\rho)} \\
&\quad + \frac{2\alpha \mathrm{V}(t-1+\rho)\mathrm{I}(t-1+\rho)}{\mathrm{V}(t-1+\rho)+\mathrm{I}(t-1+\rho)} - (\omega+\delta+\rho)\mathrm{I}(t-1+\rho) + \gamma \mathrm{R}(t-1+\rho) \Big] \\
\mathrm{R}(t) &= \mathrm{R}(0) + \frac{1}{\Gamma(\rho)} \sum_{t=1-\rho}^{t-\rho} (\nabla)^{\rho-1} \Big[ \rho \mathrm{I}(t-1+\rho) - (\delta+\gamma+\xi)\mathrm{R}(t-1+\rho) \Big].
\end{aligned} \tag{13}$$

We see that for positive initial condition, the right sides of system (13) are also positive for $t > 0$. Hence we conclude that all solution $\mathrm{S}(t) > 0$, $\mathrm{V}(t) > 0$, $\mathrm{I}(t) > 0$, and $\mathrm{R}(t) > 0$ for all $t > 0$. Thus positivity of solution for model (2) has been proved. Also the solution has been proved bounded in case of (1). In the same way, we can claim that solution of (2) is also bounded. The model (2) can be written as in equivalent form

$$\begin{aligned} {}^{C}\Delta^{\rho} z(t) &= \mathbb{F}(t-1+\rho, z(t-1+\rho)), \\ z(0) &= z_0, \end{aligned} \tag{14}$$

where $z(t) = (\mathrm{S}(t), \mathrm{V}(t), \mathrm{I}(t), \mathrm{R}(t))$, and $\mathbb{F}(t-1+\rho, z(t-1+\rho))$

$$= \begin{pmatrix} (1-\mu)\Lambda - \dfrac{2\beta \mathrm{S}((t-1+\rho)\mathrm{I}(t-1+\rho)}{\mathrm{S}(t-1+\rho)+\mathrm{I}(t-1+\rho)} - (\delta+\psi)\mathrm{S}(t-1+\rho) + \xi \mathrm{R}(t-1+\rho) + \varphi \mathrm{V}(t-1+\rho) \\ \mu\Lambda + \psi \mathrm{S}(t-1+\rho) - \dfrac{2\alpha \mathrm{V}(t-1+\rho)\mathrm{I}(t-1+\rho)}{\mathrm{V}(t-1+\rho)+\mathrm{I}(t-1+\rho)} - (\delta+\varphi)\mathrm{V}(t-1+\rho) \\ \dfrac{2\beta \mathrm{S}(t-1+\rho)\mathrm{I}(t-1+\rho)}{\mathrm{S}(t-1+\rho)+\mathrm{I}(t-1+\rho)} + \dfrac{2\alpha \mathrm{V}(t-1+\rho)\mathrm{I}(t-1+\rho)}{\mathrm{V}(t-1+\rho)+\mathrm{I}(t-1+\rho)} - (\omega+\delta+\rho)\mathrm{I}(t-1+\rho) + \gamma \mathrm{R}(t-1+\rho) \\ \rho \mathrm{I}(t-1+\rho) - (\delta+\gamma+\xi)\mathrm{R}(t-1+\rho) \end{pmatrix}.$$

Thank to Theorem 3.6, the problem (14) yields

$$z(t) = z(0) + \sum_{k=0}^{t-\rho} \frac{(t-s-1)^{\rho-1}}{\Gamma(\rho)} \mathbb{F}(k+\rho-1, z(k+\rho-1)). \tag{15}$$

The space described by

$$\mathbb{X} = [\rho-1, b+\rho]_{\mathbf{N}_{\rho-1}} \times [\rho-1, b+\rho]_{\mathbf{N}_{\rho-1}} \times [\rho-1, b+\rho]_{\mathbf{N}_{\rho-1}} \times [\rho-1, b+\rho]_{\mathbf{N}_{\rho-1}},$$

and $\{z(t)\}_{t=\rho-1}^{b+\rho}$, under the norm $\|z\| = \sup_{t\in[\rho-1, b+\rho]_{\mathbf{N}_{\rho-1}}} |z(t)|$. State some hypothesis as bellow:

$(H_1)$ For continuous $\mathbb{F}$ with $z, \hat{z} \in \mathbb{X}$, one has

$$|\mathbb{F}(t, z) - \mathbb{F}(t, \hat{z})| \leq \mathscr{L}_{\mathbb{F}} |z - \hat{z}|, \ \mathscr{L}_{\mathbb{F}} > 0.$$

$(H_2)$ The nonlinear function $\mathbb{F}$ obeys

$$|\mathbb{F}(t, z(t))| \leq \mathscr{C}_{\mathbb{F}} |z| + \mathbb{D}, \ \text{where } \mathscr{C}_{\mathbb{F}} > 0, \ \mathbb{D} > 0.$$

Also we use

$$\widehat{A} = \max\left\{\frac{\Gamma(t+1)}{\Gamma(\rho+1)\Gamma(t-\rho+1)}\right\} = \frac{\Gamma(\rho+b+1)}{\Gamma(\rho+1)\Gamma(\rho+1)}.$$

**Theorem 4.1** For model (2) there will be at least one solution under the hypothesis $(H_2)$ if $\mathbb{C}_{\mathbb{F}}\widehat{A} < 1$ holds.

**Proof.** Consider a closed and convex subset $\mathbb{C}$ of $\mathbb{X}$ described by $\mathbb{C} = \{z \in \mathbb{X} : \|z\| \leq r\}$, where $r \geq \dfrac{z(0) + \mathbb{D}\widehat{A}}{1 - \mathbb{C}_{\mathbb{F}}\widehat{A}}$. Let define $\Theta : \mathbb{C} \to \mathbb{C}$ by

$$\Theta z(t) = z(0) + \frac{1}{\Gamma(\rho)}\sum_{k=0}^{t-\rho}(\nabla)^{\rho-1}\mathbb{F}(k+\rho-1, z(k+\rho-1)). \tag{16}$$

Take $z \in \mathbb{C}$, we have

$$\begin{aligned}
&|\Theta z(t)| \\
&= \left| z(0) + \frac{1}{\Gamma(\rho)}\sum_{k=0}^{t-\rho}(\nabla)^{\rho-1}\mathbb{F}(k+\rho-1, z(k+\rho-1))\right| \\
&= z(0) + \frac{1}{\Gamma(\rho)}\sum_{k=0}^{t-\rho}\left|(\nabla)^{\rho-1}\mathbb{F}(k+\rho-1, z(k+\rho-1))\right| \\
&\leq z(0) + \frac{1}{\Gamma(\rho)}\sum_{k=0}^{t-\rho}|(\nabla)^{\rho-1}||\mathbb{F}(k+\rho-1, z(k+\rho-1))| \\
&\leq z(0) + \frac{1}{\Gamma(\rho)}\sum_{k=0}^{t-\rho}[\mathscr{C}_{\mathbb{F}}\|z\| + \mathbb{D}]\,|(\nabla)^{\rho-1}| \\
&\leq z(0) + [\mathscr{C}_{\mathbb{F}}r + \mathbb{D}]\max\frac{1}{\Gamma(\rho)}\sum_{k=0}^{t-\rho}|(\nabla)^{\rho-1}| \\
&\leq z(0) + [\mathscr{C}_{\mathbb{F}}r + \mathbb{D}]\widehat{A} \leq r.
\end{aligned} \tag{17}$$

From (17), we conclude that $\Theta z \in \mathbb{C}$ which implies that $\Theta$ maps $\mathbb{C}$ to $\mathbb{C}$. Also this shows that $\Theta$ is bounded and using Theorem 3.8, the result holds. □

**Theorem 4.2** The model (2) has a unique solution under the hypothesis $(H_1)$ if $\dfrac{\mathscr{L}_{\mathbb{F}}\widehat{A}}{\Gamma(\rho)} < 1$ holds.

**Proof.** Take $z$, $\hat{z} \in \mathbb{X}$, then we have

$$
\begin{aligned}
&\|\Theta z - \Theta \hat{z}\| \\
&= \sup_{t\in[\rho-1,\, b+\rho]_{\mathbf{N}_{\rho-1}}} |\Theta z(t) - \Theta \hat{z}(t)| \\
&= \sup_{t\in[\rho-1,\, b+\rho]_{\mathbf{N}_{\rho-1}}} \left| \frac{1}{\Gamma(\rho)} \sum_{k=0}^{t-\rho} (\nabla)^{\rho-1} \mathbb{F}(k+\rho-1, z(k+\rho-1)) - \frac{1}{\Gamma(\rho)} \sum_{k=0}^{t-\rho} (\nabla)^{\rho-1} \mathbb{F}(k+\rho-1, \hat{z}(k+\rho-1)) \right| \\
&\leq \sup_{t\in[\rho-1,\, b+\rho]_{\mathbf{N}_{\rho-1}}} \frac{1}{\Gamma(\rho)} \sum_{k=0}^{t-\rho} (\nabla)^{\rho-1} |\mathbb{F}(k+\rho-1, z(k+\rho-1)) - \mathbb{F}(k+\rho-1, \hat{z}(k+\rho-1))| \\
&\leq \sup_{t\in[\rho-1,\, b+\rho]_{\mathbf{N}_{\rho-1}}} \frac{1}{\Gamma(\rho)} \sum_{k=0}^{t-\rho} (\nabla)^{\rho-1} \mathscr{L}_{\mathbb{F}} \|z - \hat{z}\| \\
&= \frac{\mathscr{L}_{\mathbb{F}} \|z - \hat{z}\|}{\Gamma(\rho)} \sup_{t\in[\rho-1,\, b+\rho]_{\mathbf{N}_{\rho-1}}} \sum_{k=0}^{t-\rho} (\nabla)^{\rho-1} \\
&= \frac{\mathscr{L}_{\mathbb{F}} \widehat{A}}{\Gamma(\rho)} \|z - \hat{z}\|. \qquad (18)
\end{aligned}
$$

Hence, we see that $\Theta$ fulfills the conditions of contraction in (18). Hence due to Banach Theorem [40], the model (2) has a unique solution. □

**Remark 4.3** Since contraction theorem holds for the given problem (2), therefore on using retraction-displacement condition [41], the solution is also U-H stable.

## 4.1 *Computation of DFE point and $\mathscr{R}_{v,0}$, $\mathscr{R}_0$*

We compute the DFE and EE points of model (2) and also the use the next generation matrix theory to obtain the reproductive number $\mathscr{R}_0$. From system (2), we have by using $\mathrm{R} = \mathrm{I} = 0$, to calculate DFE $E^0 = \left(\mathrm{S}^0, \mathrm{V}^0, \mathrm{I}^0, \mathrm{R}^0\right)$, where $\mathrm{R}^0 = 0$, $\mathrm{I}^0 = 0$ and

$$
\mathrm{S}^0 = \frac{\Lambda(\delta + \varphi - \mu\delta)}{\delta(\delta + \varphi + \psi)}, \; \mathrm{V}^0 = \frac{\Lambda(\delta\mu + \psi)}{\delta(\delta + \varphi + \psi)}.
$$

We use the next generation matrix theory [42] to derivative $\mathscr{R}_0$. Considering the Equation (1) and Equation (3) of model (2), using next generation matrix method, we obtain

$$X = \begin{pmatrix} 0 & \dfrac{-2\beta}{S^0} \\ 0 & \dfrac{2\beta}{S^0} + 2\alpha \end{pmatrix}, \; Y = \begin{pmatrix} \dfrac{1}{(\omega+\delta+\rho)} & 0 \\ 0 & \dfrac{1}{\delta+\psi} \end{pmatrix}.$$

Further, we have from matrices $X$ and $Y$

$$XY^{-1} = \begin{pmatrix} 0 & \dfrac{-2\beta}{S^0(\delta+\psi)} \\ 0 & \dfrac{2\beta + 2S^0\alpha}{S^0(\delta+\psi)} \end{pmatrix}.$$

Hence, the maximum eigen value of $\det(XY^{-1}) = \dfrac{2\beta + 2S^0\alpha}{S^0(\delta+\psi)}$. After simplification by using value of $S^0$, we get

$$\mathscr{R}_{v,0} = \frac{2[\alpha\Lambda(\delta+\varphi-\mu\delta)+\beta\delta(\delta+\varphi+\omega)]}{\Lambda(\varphi+\delta-\mu\delta)}.$$

Here if there is no vaccination process, then $\mu = 0$, then one has

$$\mathscr{R}_0 = \frac{2[\alpha\Lambda(\delta+\varphi)+\beta\delta(\delta+\varphi+\omega)]}{\Lambda(\varphi+\delta)}.$$

Here, we discuss the sensitivity of the concerned numbers in the following Table 1 using the values from Table 2. We use the formula $\$_q^{\mathscr{R}_{v,0}} = \dfrac{q}{\mathscr{R}_{v,0}} \dfrac{\partial \mathscr{R}_{v,0}}{\partial q}$, where $q$ means parameters.

From Table 1, we see that an 100% increase in $\alpha$, $\omega$ will produces 99% impact on the corresponding reproductive number $\mathscr{R}_{v,0}$. The other parameters has very low impact on the value of $\mathscr{R}_{v,0}$. In the same way, the 100% increase in values of $\alpha$ will produce the impact of 100% on the value of $\mathscr{R}_0$. The corresponding bar graphs for both the quantities are presented in Figures 3 and 4 respectively.

**Table 1.** Sensitivity indices of $\mathscr{R}_{v,0}$ and $\mathscr{R}_0$

| Sensitivity index for $\mathscr{R}_{v,0}$ | Value | Sensitivity index for $\mathscr{R}_0$ | Value |
|---|---|---|---|
| $\$_\alpha^{\mathscr{R}_{v,0}}$ | 0.99915525 | $\$_\alpha^{\mathscr{R}_0}$ | 1 |
| $\$_\beta^{\mathscr{R}_{v,0}}$ | 0.000004251 | $\$_\beta^{\mathscr{R}_0}$ | 0.0000425454 |
| $\$_\omega^{\mathscr{R}_{v,0}}$ | 0.0000024561053 | $\$_\omega^{\mathscr{R}_0}$ | 0.00000245818 |
| $\$_\delta^{\mathscr{R}_{v,0}}$ | 0.00000016200 | $\$_\delta^{\mathscr{R}_0}$ | 0.00000424445 |
| $\$_\varphi^{\mathscr{R}_{v,0}}$ | −0.00000015532 | $\$_\varphi^{\mathscr{R}_0}$ | −0.0000001549 |
| $\$_\mu^{\mathscr{R}_{v,0}}$ | 0.0000000000633 | $\$_\Lambda^{\mathscr{R}_0}$ | −0.00000424809 |
| $\$_\Lambda^{\mathscr{R}_{v,0}}$ | −0.0000042494 | | |

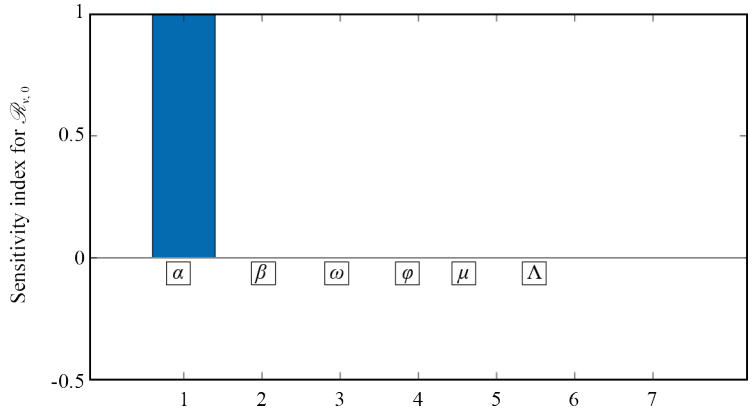


**Figure 3.** Sensitivity analysis of $\mathscr{R}_{v,0}$

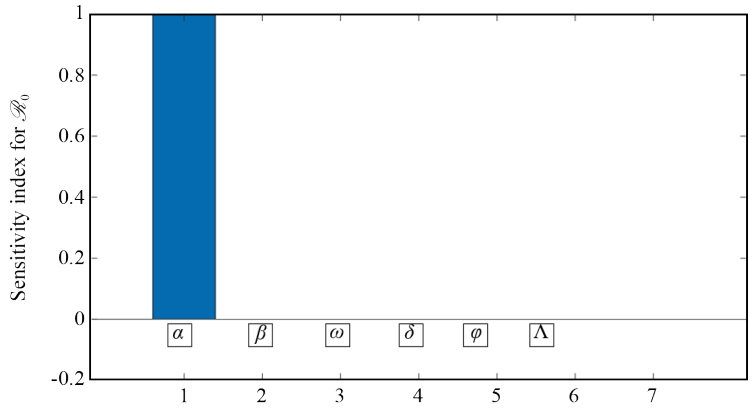


**Figure 4.** Sensitivity analysis of $\mathscr{R}_0$

## 5. Numerical tool to evaluate the model (2)

This portion is devoted to present numerical analysis of model (2). setting $t-\rho=i$ and inview of (13) and Remark 3.7, from (12), one has

$$\mathrm{S}(n)=\mathrm{S}(0)+\frac{1}{\Gamma(\rho)}\sum_{i=1}^{n}\frac{(n+\rho-i)}{\Gamma(n-i+1)}\Big[(1-\mu)\Lambda-\frac{2\beta\mathrm{S}((i-1)\mathrm{I}(i-1)}{\mathrm{S}(i-1)+\mathrm{I}(i-1)}-(\delta+\psi)\mathrm{S}(i-1)$$

$$+\xi\mathrm{R}(i-1)+\varphi\mathrm{V}(i-1)\Big]$$

$$\mathrm{V}(t)=\mathrm{V}(0)+\frac{1}{\Gamma(\rho)}\sum_{i=1}^{n}\frac{(n+\rho-i)}{\Gamma(n-i+1)}\Big[\mu\Lambda+\psi\mathrm{S}(i-1)-\frac{2\alpha\mathrm{V}(i-1)\mathrm{I}(i-1)}{\mathrm{V}(i-1)+\mathrm{I}(i-1)}-(\delta+\varphi)\mathrm{V}(i-1)\Big]$$

$$\mathrm{I}(t)=\mathrm{I}(0)+\frac{1}{\Gamma(\rho)}\sum_{i=1}^{n}\frac{(n+\rho-i)}{\Gamma(n-i+1)}\Bigg[\mathrm{I}(0)+\frac{2\beta\mathrm{S}(i-1)\mathrm{I}(i-1)}{\mathrm{S}(i-1)+\mathrm{I}(i-1)}$$

$$+\frac{2\alpha\mathrm{V}(i-1)\mathrm{I}(i-1)}{\mathrm{V}(i-1)+\mathrm{I}(i-1)}-(\omega+\delta+\rho)\mathrm{I}(i-1)+\gamma\mathrm{R}(i-1)\Bigg]$$

$$\mathrm{R}(t)=\mathrm{R}(0)+\frac{1}{\Gamma(\rho)}\sum_{i=1}^{n}\frac{(n+\rho-i)}{\Gamma(n-i+1)}\Big[\rho\mathrm{I}(i-1)-(\delta+\gamma+\xi)\mathrm{R}(i-1)\Big]. \tag{19}$$

Here, the model (19) is a discrete type SVIR type model that involve memory effects along with vaccination class. Also, the state variables $\mathrm{S}(n)$, $\mathrm{V}(n)$, $\mathrm{I}(n)$, and $\mathrm{R}(n)$ depend on their previous values that is $\mathrm{S}(0)$, $\mathrm{V}(0)$, $\mathrm{I}(0)$, $\mathrm{R}(0)$, etc.

## 5.1 *Parameters estimation*

To estimate the parameters, let take the initial values from [42] as

$$\mathrm{S}(0)=101{,}368{,}369,\quad \mathrm{V}(0)=125{,}000{,}000,\quad \mathrm{I}(0)=1{,}581{,}936,\quad \mathrm{R}(0)=1{,}538{,}689.$$

According to the source [42], till date the total individuals who were vaccinated against COVID-19 are 125,000,000 of total population 229,488,994. Here, $\Lambda=\mu*N(0)$, as $N(0)$ is the initial total population of the country. The parameters values, here we have given as in Table 2 collected from literature and some were assumed.

**Table 2.** Parameters numerical values of considered model

| Symbol | Numerical value | Reference | Symbol | Numerical value | Reference |
|---|---|---|---|---|---|
| $\Lambda$ | $\frac{229{,}488{,}994}{59\times 365}$ | [43] | $\mu$ | $\frac{1}{67.7\times 365}$ | [43] |
| $\psi$ | 0.54 | Estimated | $\beta$ | 0.3 | [43] |
| $\delta$ | $\frac{7.021}{1{,}000}$ | [43] | $\omega$ | 0.026 | [43] |
| $\rho$ | 0.19 | [43] | $\gamma$ | 0.05 | Estimated |
| $\xi$ | 0.0123 | Estimated | $\alpha$ | 0.11 | Estimated |
| $\varphi$ | 0.012 | Estimated | | | |

Using the numerical values mentioned above in Table 2 and the initial values, we present the graphical illustration for various fractional orders in Figures 5-8 respectively.

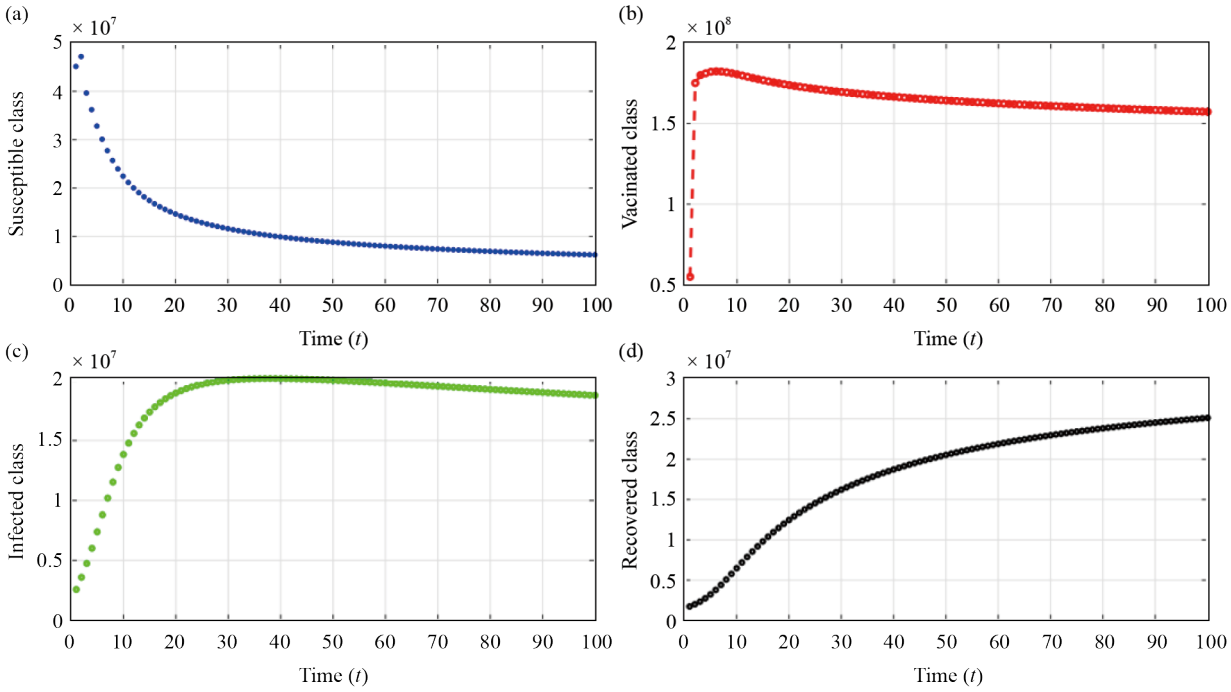


**Figure 5.** Graphical presentation for the model (2) at $\rho = 0.50$ for various compartments

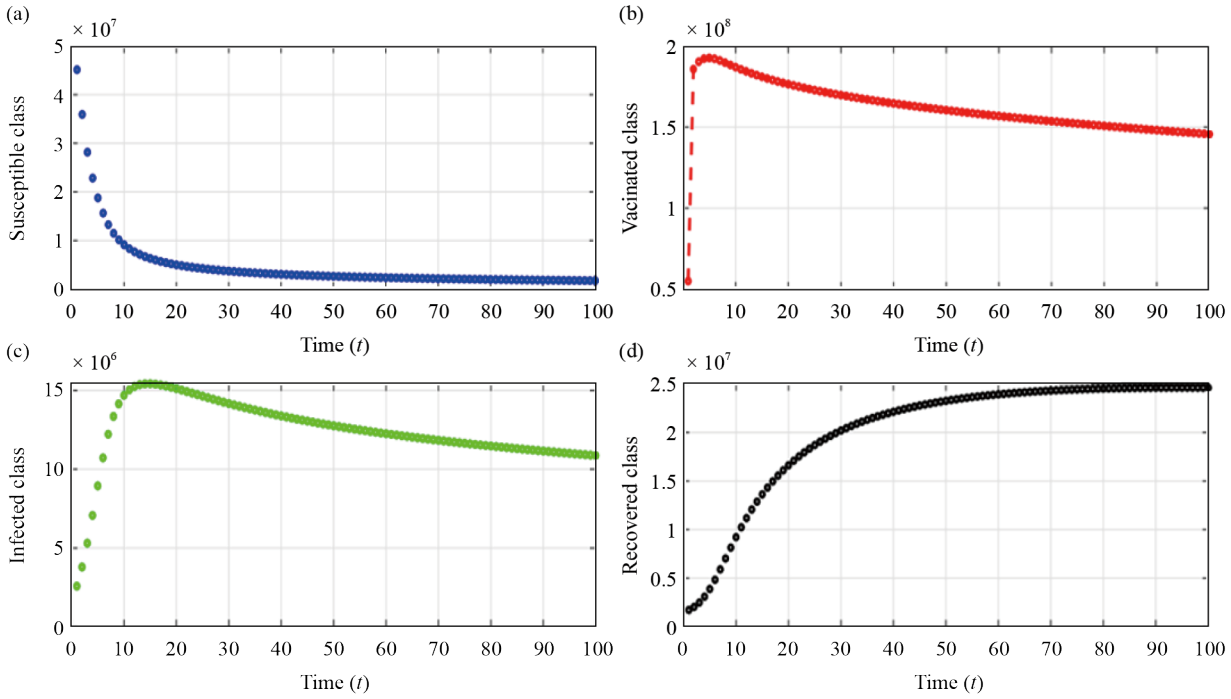


**Figure 6.** Graphical presentation for the model (2) at $\rho = 0.70$ for various compartments

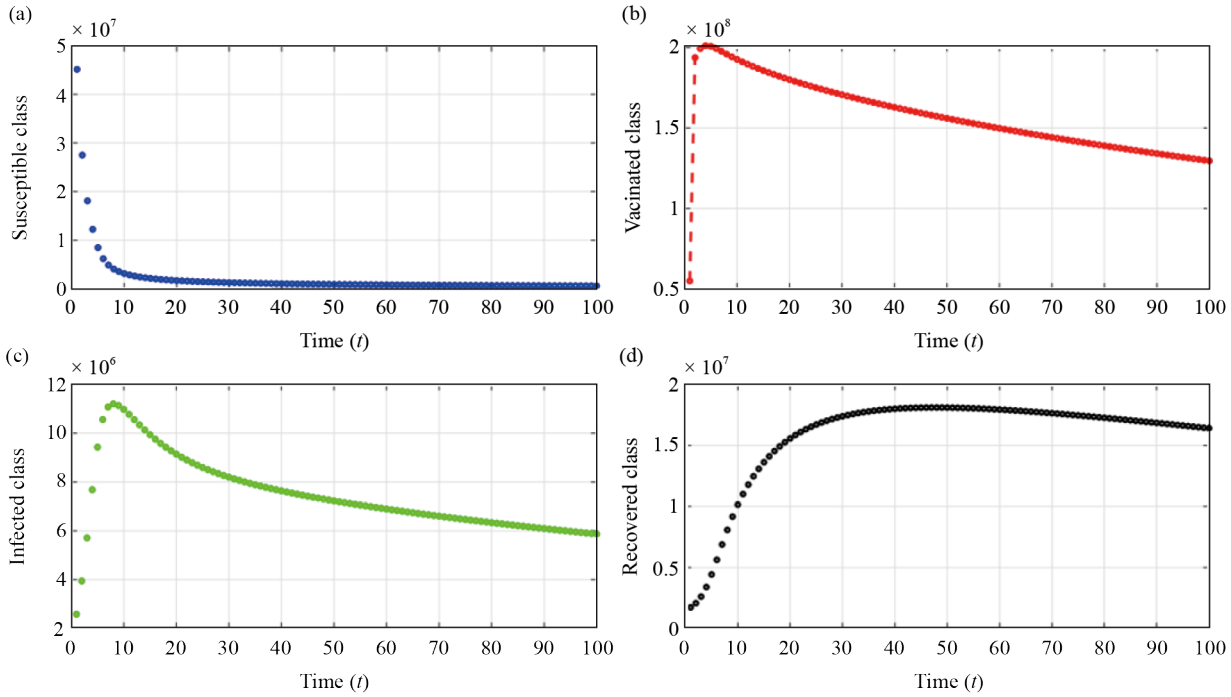


**Figure 7.** Graphical presentation for the model (2) at $\rho = 0.85$ for various compartments

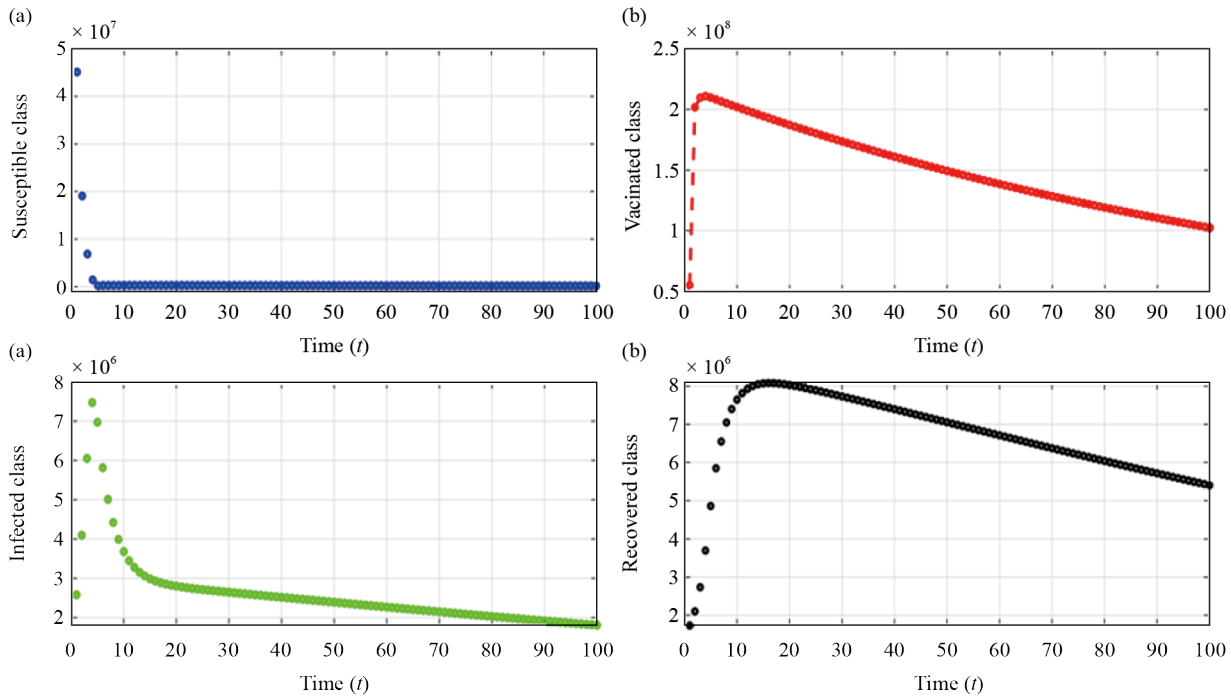


**Figure 8.** Graphical presentation for the model (2) at $\rho = 1.00$ for various compartments

From Figures 5-8a presents the dynamical behaviour of susceptible class for 100 days using different fractional orders. The population is declining as the time passes because of the spread of infection in the community. In the mean time, from Figures 5-8b, we deduce the dynamics of vaccinated class which first show increase and some time after become stable.

Also, Figures 5-8c presents the dynamics of infected class against various fractional orders values. In addition, Figures 5-8d presents the dynamics of recovered class. As compared to traditional derivatives models, the discrete type models are more realistic and efficient, because the available data of peltation in such cases is always discrete. Here, in Figure 9, we have compared the real data and simulated discrete solution using the data of [44]. We see both plots closely agree.

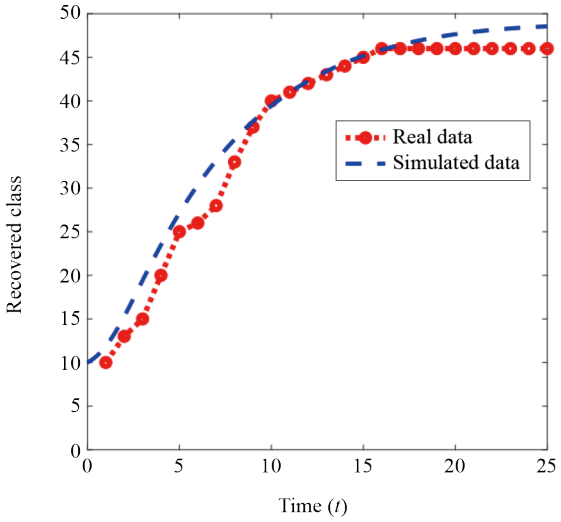


**Figure 9.** Comparison between real and simulated data for recovered class using integer order

## 6. ANNs analysis of the presented model (2)

We include results based on ANNs analysis. Here, we compute some metrics for analyzing the performance and efficiency of our considered numerical algorithm and ANNs. The given formula is used to compute the MSE which is one of the fundamental metric in machine learning:

$$\text{MSE} = \frac{1}{K}\sum_{j=1}^{K}\left(Y_j - \hat{Y}_j\right)^2, \tag{20}$$

such that $K$ uses for total number of data points, $Y_j$ is the actual or numerical data point generated from our numerical algorithm and $\hat{Y}_j$ stands for predicted value by ANNs. With the help of the formula (20), we can analysis how closely our numerical data is related with the predicted value. Also, the said formula facilitates optimization procedure including gradient, variance $(\sigma)$ and standard deviation $(\mu)$ for model training. In addition, the said formula is used as a loss function in regression analysis which help in guiding the learning process for minimization of predicting error. Effective use of MSE can enhance the efficiency of performance of regression analysis. In addition, the following RMSE formula can also b e used as a fundamental tool to measure the quality of prediction.

$$\text{RMSE} = \sqrt{\frac{\sum_{j=1}^{K}\|Y_j - \hat{Y}_j\|^2}{K}}. \tag{21}$$

Here, we have presented the circuit diagram in Figure 10 that how the ANNs work by taking single input process through multi hidden layers and produce single output.

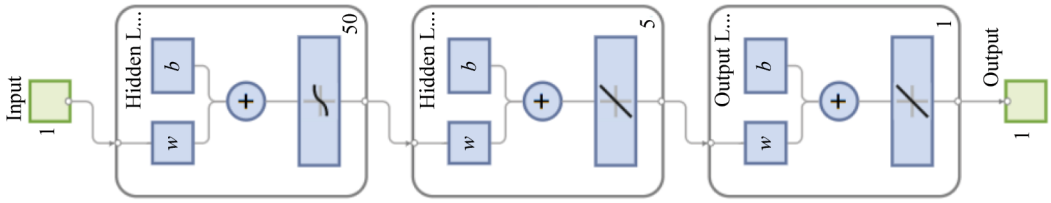


**Figure 10.** Diagrammatical presentation of ANNs

Now, we present, the corresponding analysis including performance analysis, training data, test data and validation data for all compartments in the following four sets of Figures 11-16, Figures 17-22, Figures 23-28, and Figures 29-34 respectively. Here, we have used 55 hidden layers including input and output layers for each compartment analysis.

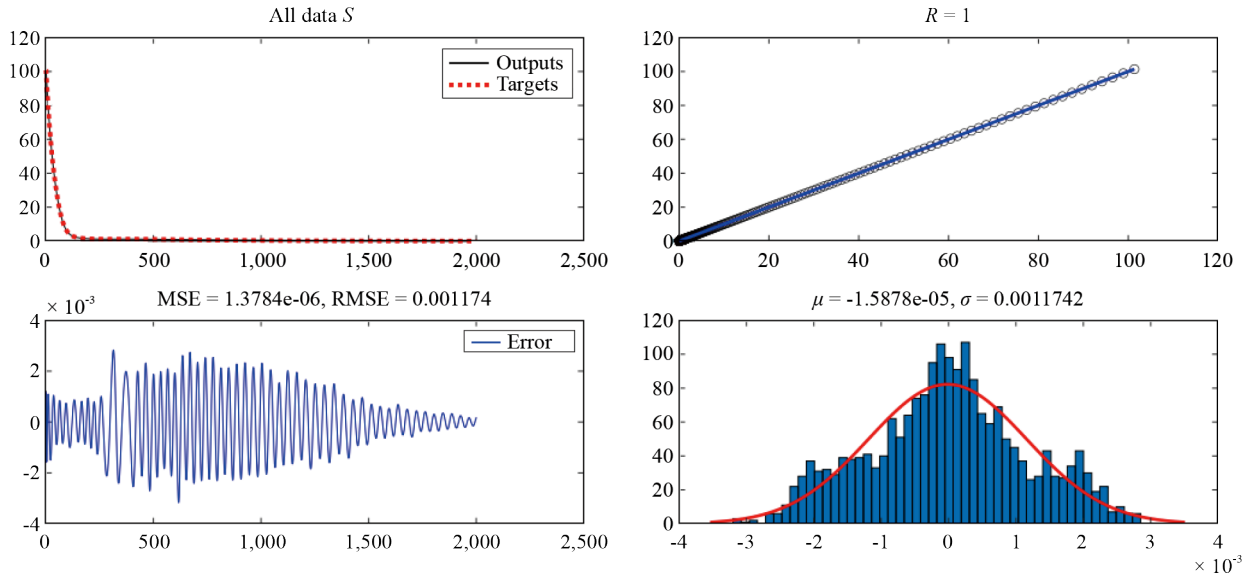


**Figure 11.** Graphical illustration of all data

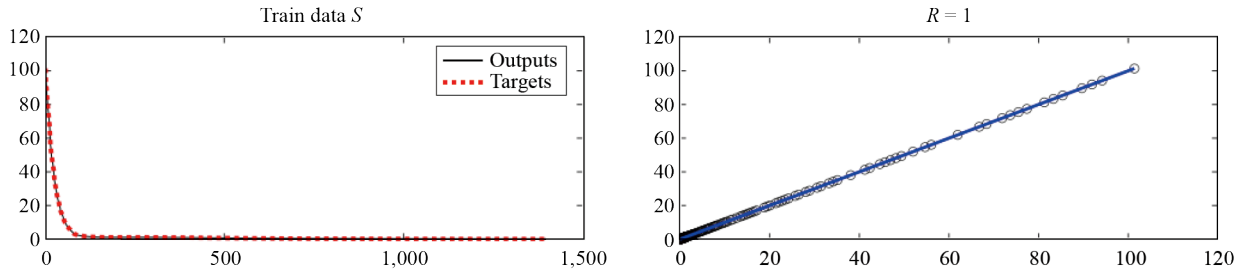

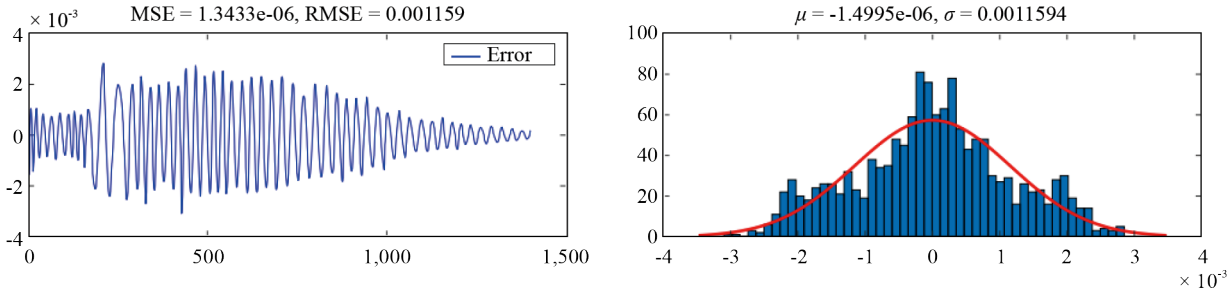


**Figure 12.** Graphical illustration of train data

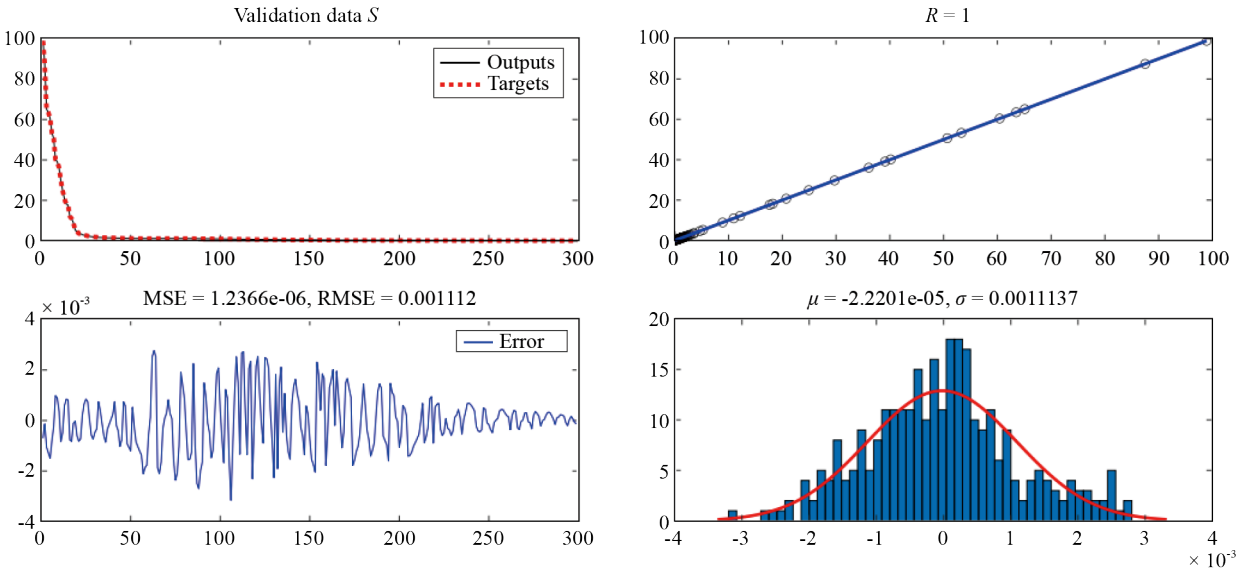


**Figure 13.** Graphical illustration of validation data

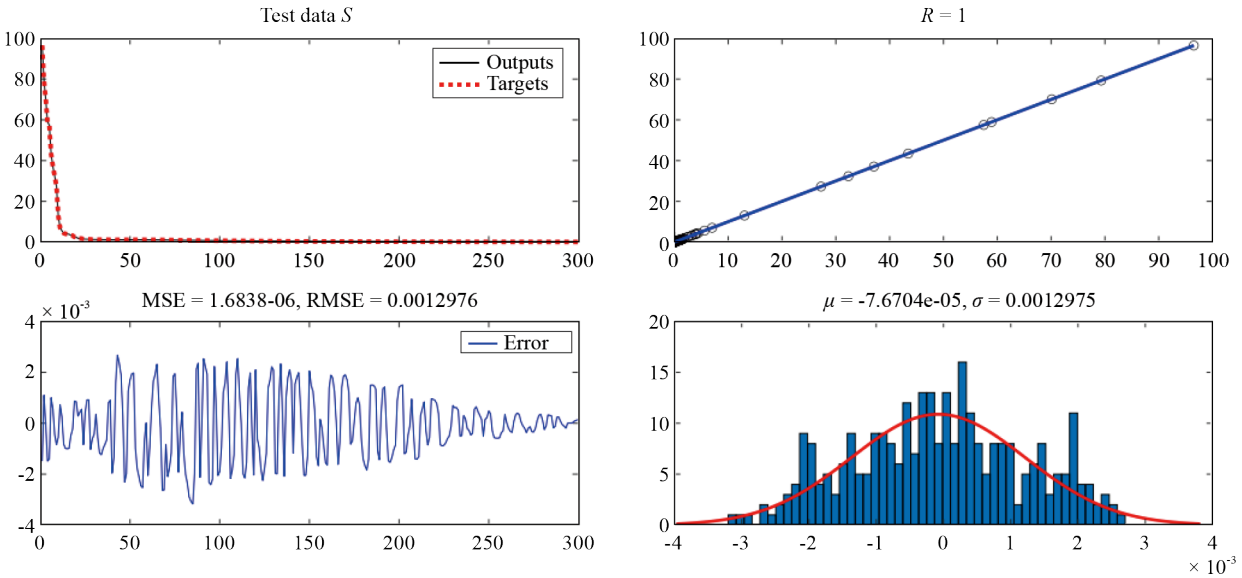


**Figure 14.** Graphical illustration of test data

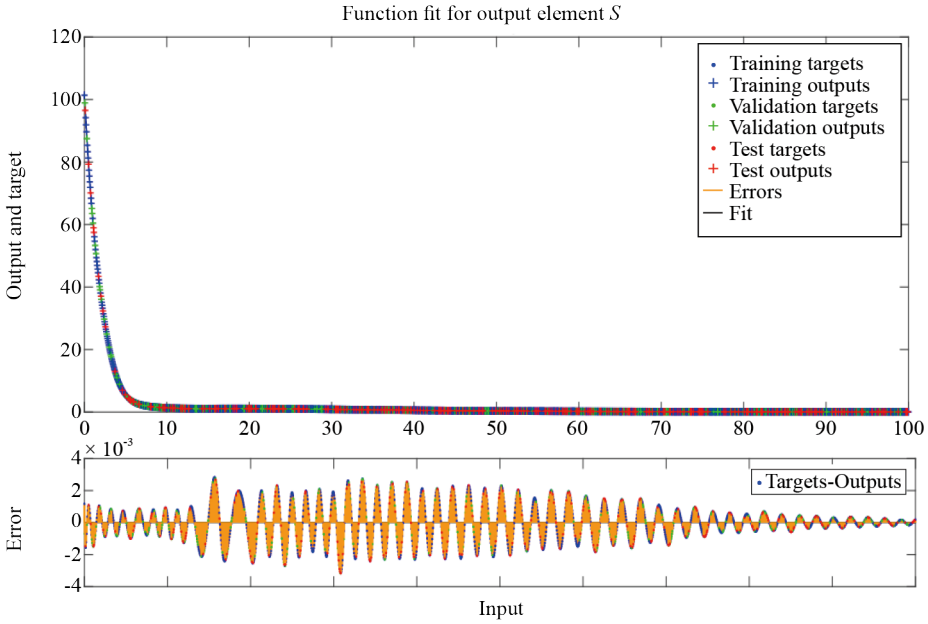


**Figure 15.** Graphical illustration of best function fit for data of *S*

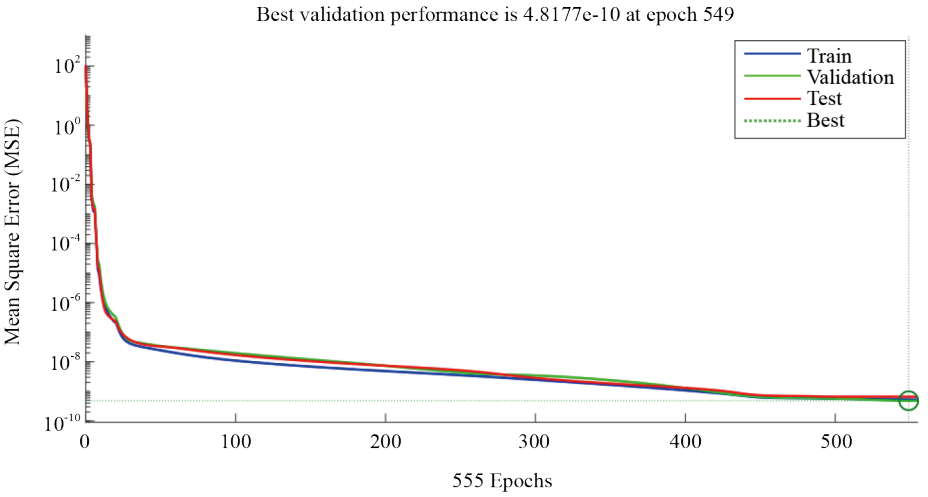


**Figure 16.** Graphical illustration of performance analysis using ANNs

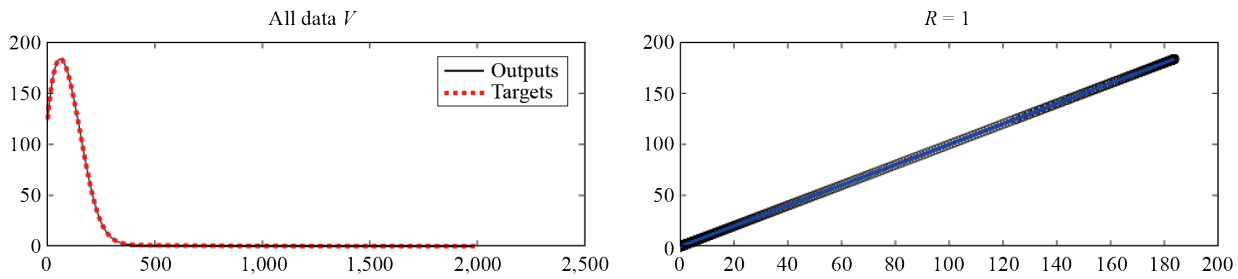

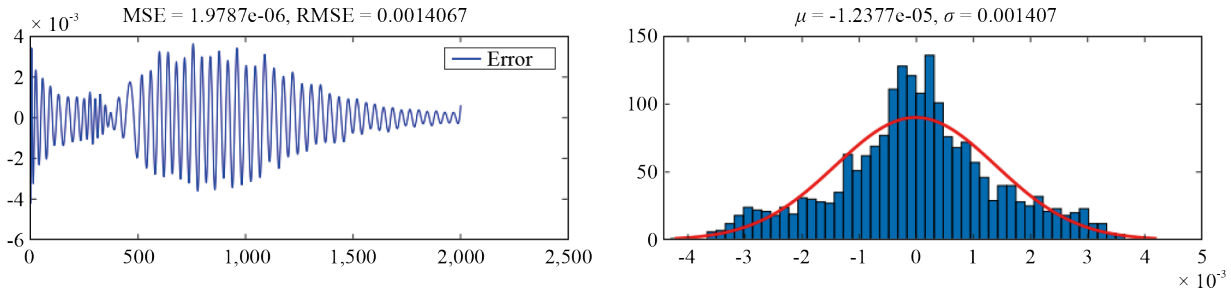


**Figure 17.** Graphical illustration of all data

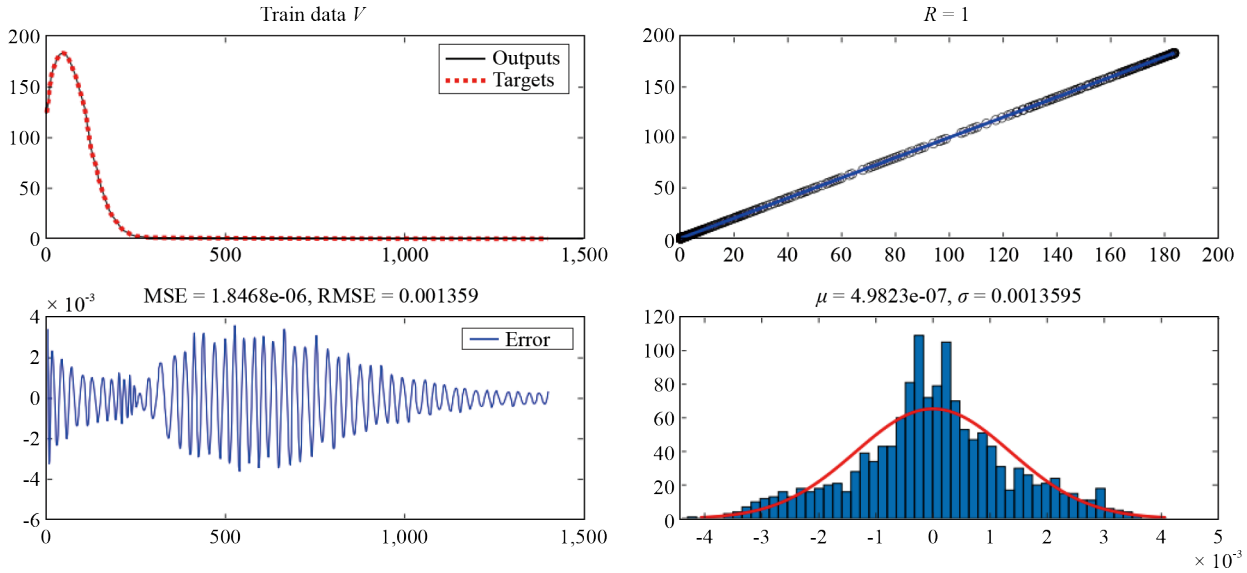


**Figure 18.** Graphical illustration of train data

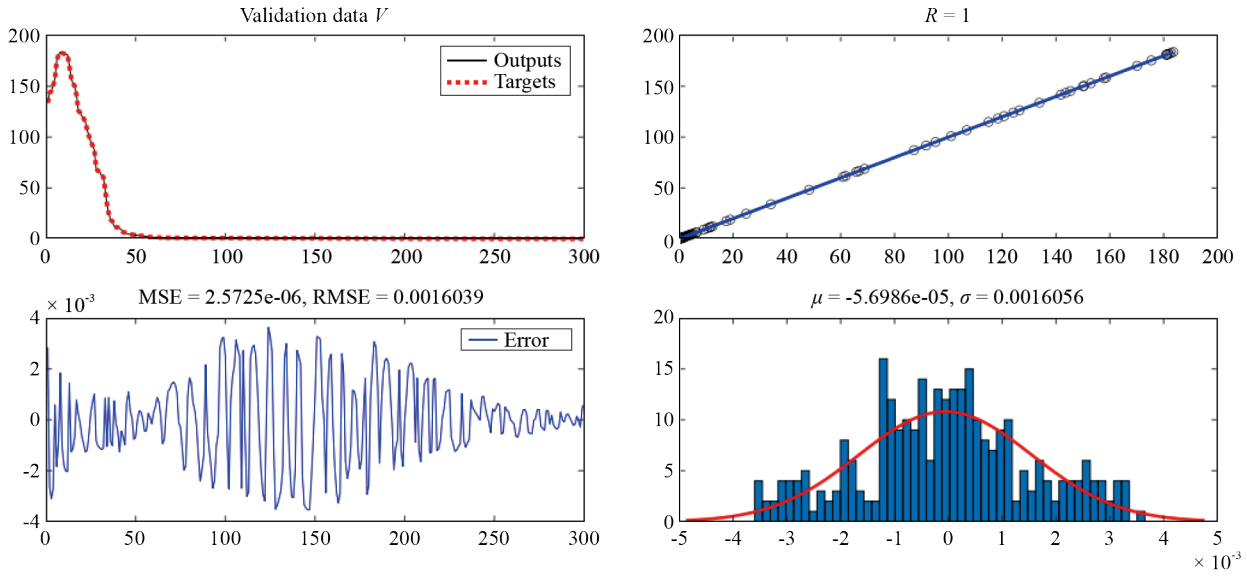


**Figure 19.** Graphical illustration of validation data

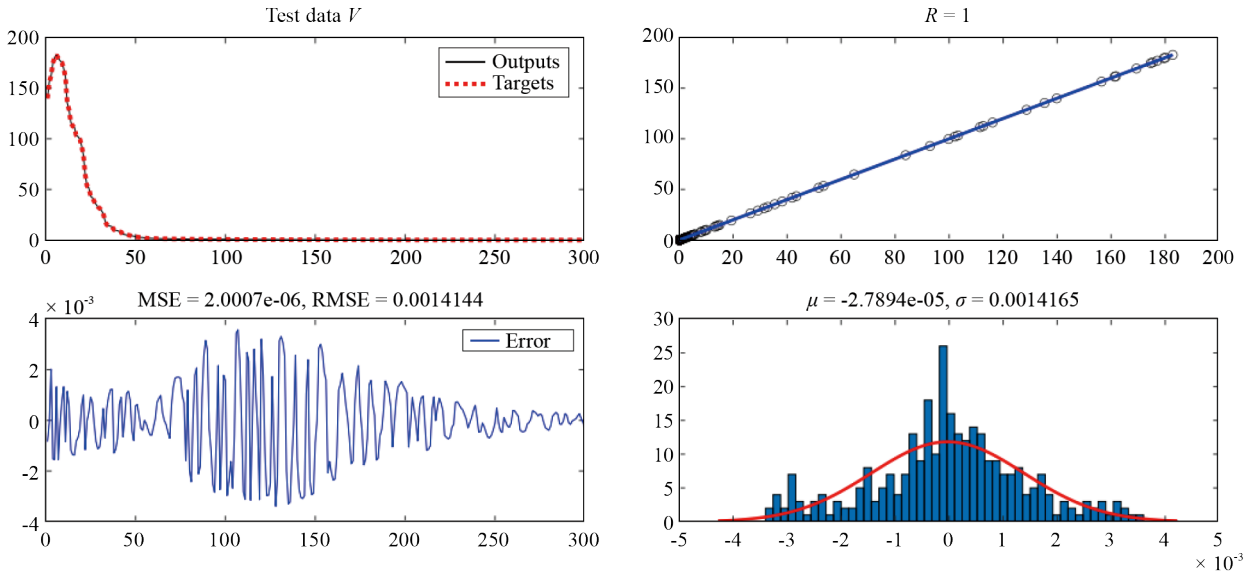


**Figure 20.** Graphical illustration of test data

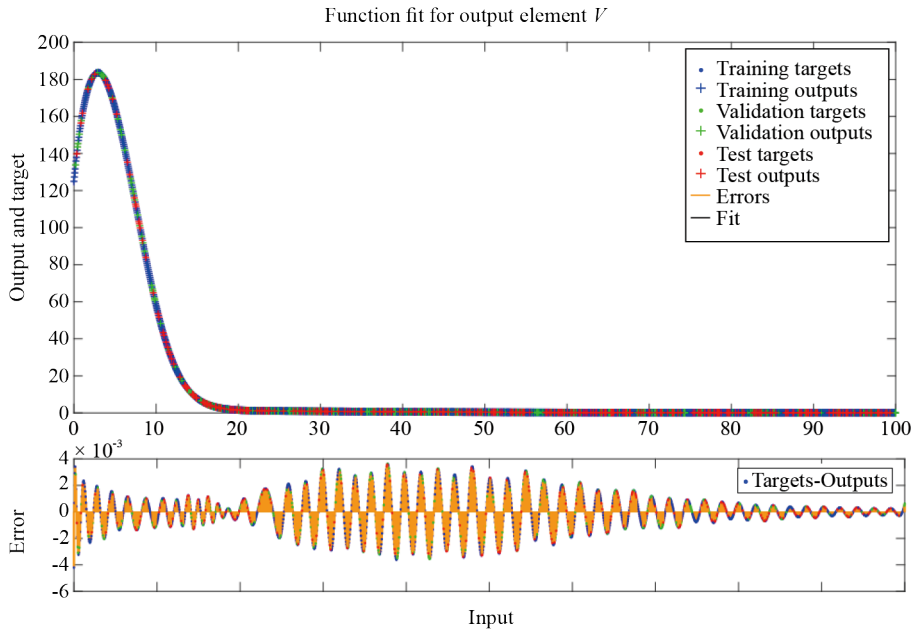


**Figure 21.** Graphical illustration of best function fit for data of $V$

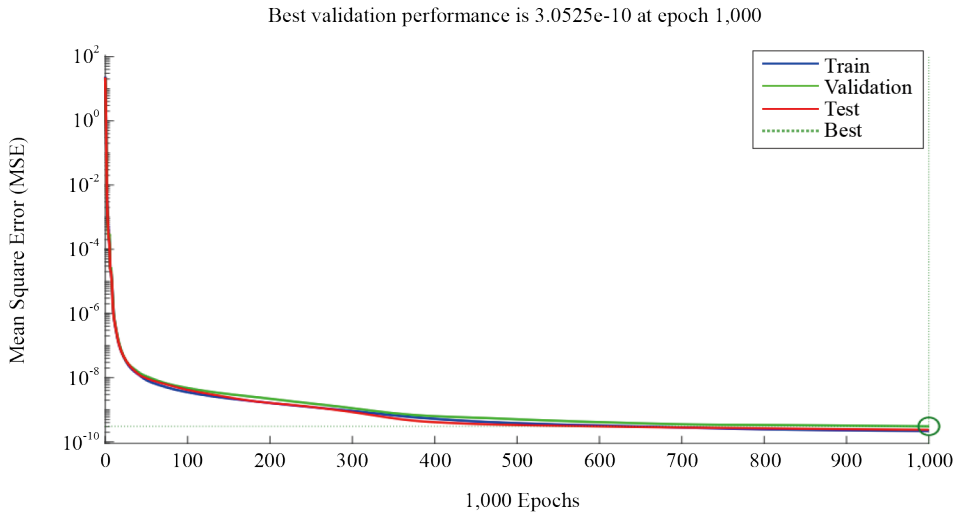


**Figure 22.** Graphical illustration of performance analysis using ANNs

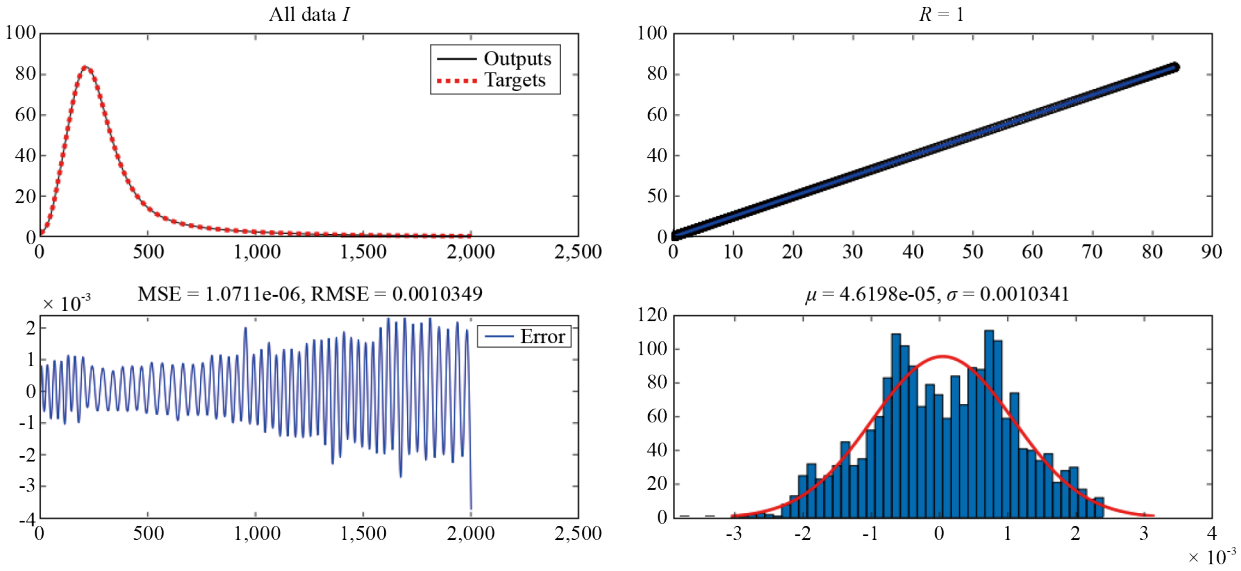


**Figure 23.** Graphical illustration of all data

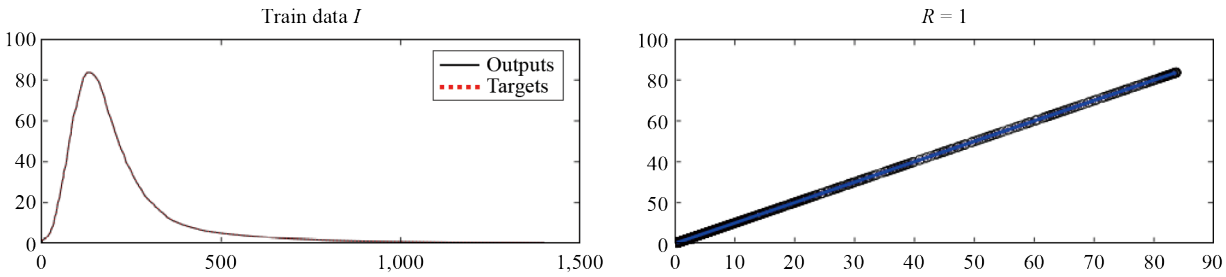

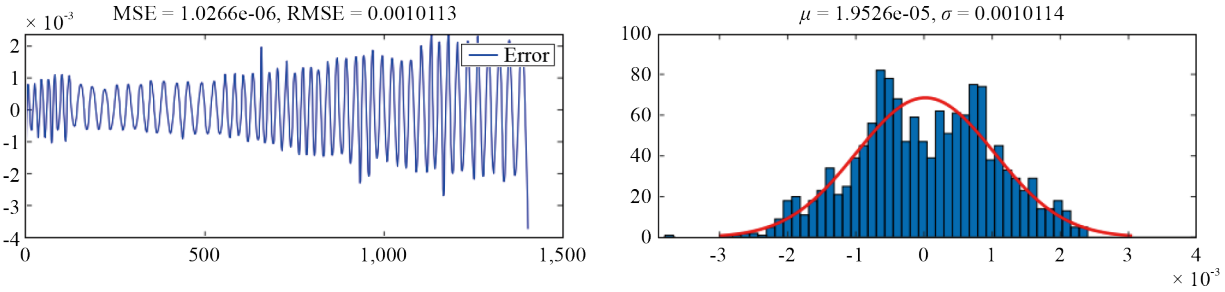


**Figure 24.** Graphical illustration of train data

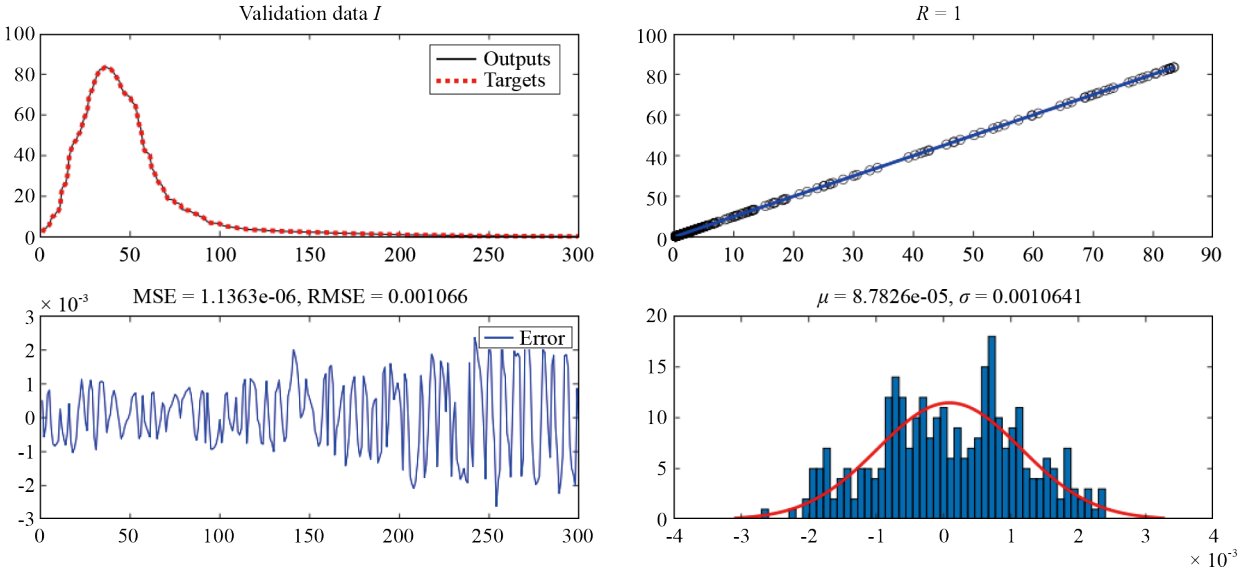


**Figure 25.** Graphical illustration of validation data

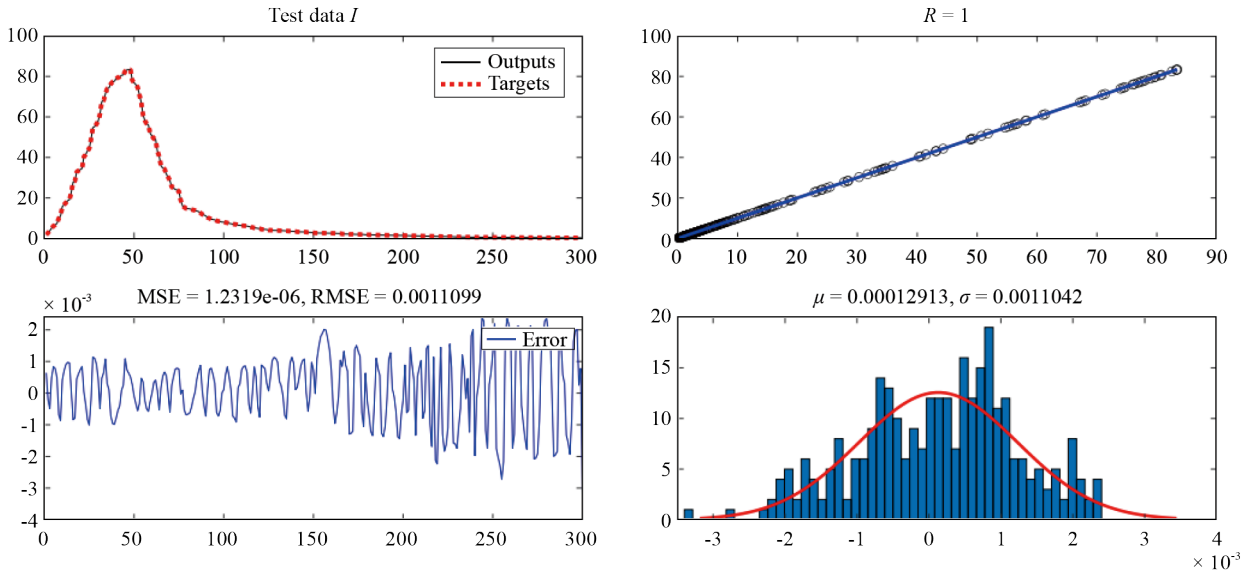


**Figure 26.** Graphical illustration of test data

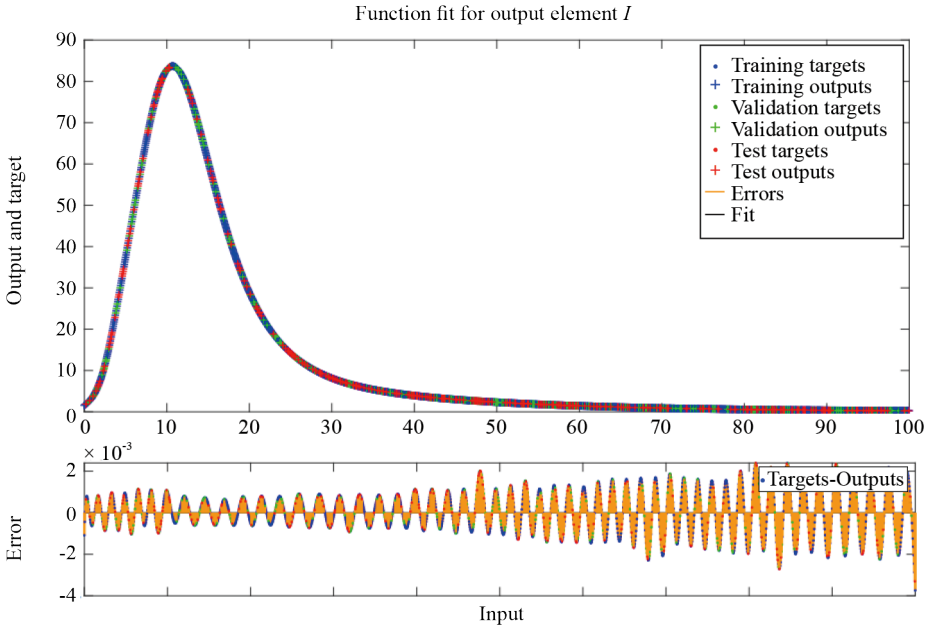


**Figure 27.** Graphical illustration of best function fit for data of $I$

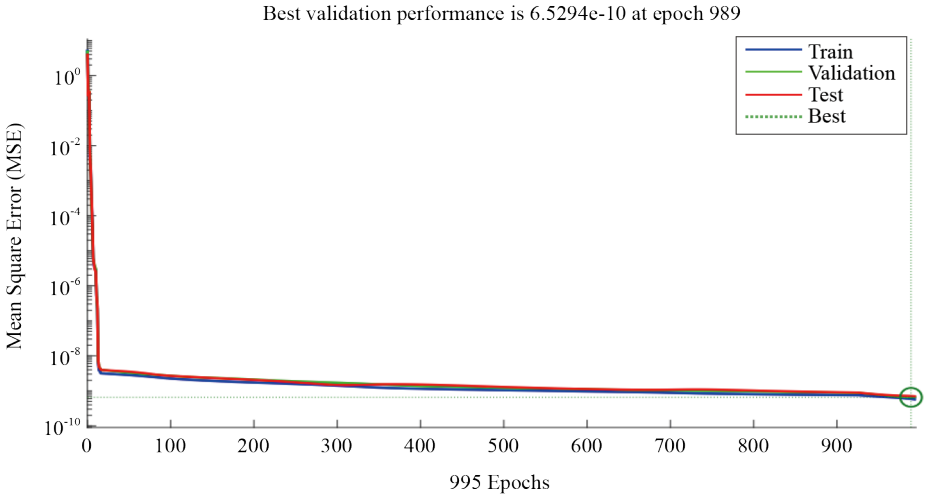


**Figure 28.** Graphical illustration of performance analysis using ANNs

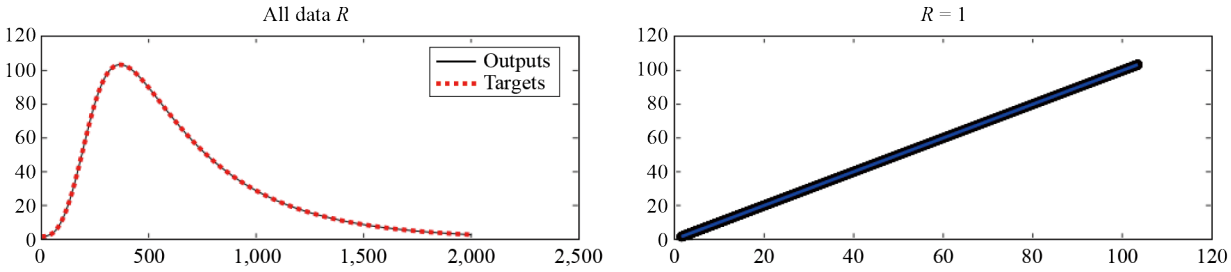

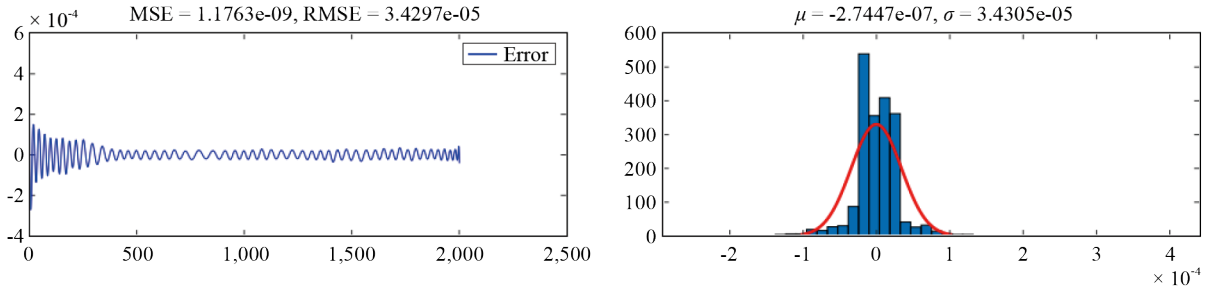


**Figure 29.** Graphical illustration of all data

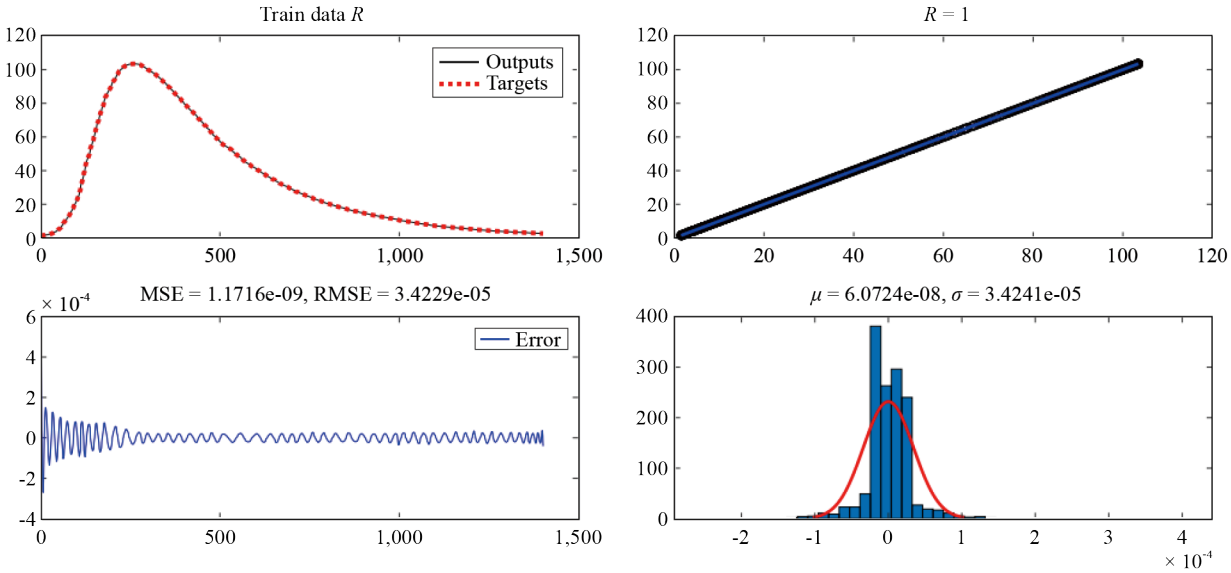


**Figure 30.** Graphical illustration of train data

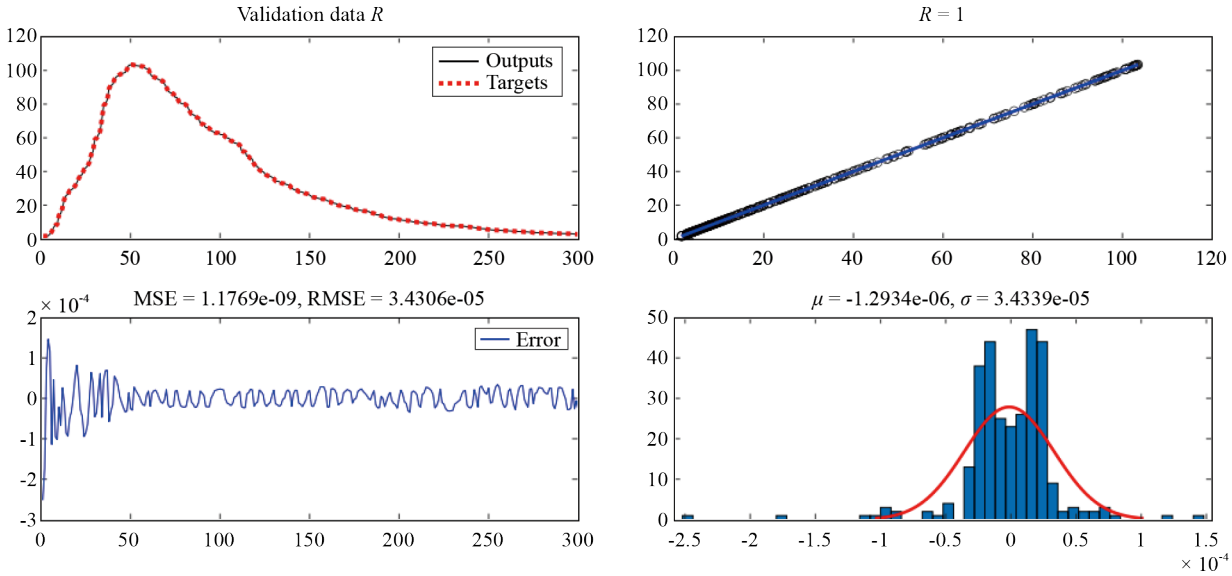


**Figure 31.** Graphical illustration of validation data

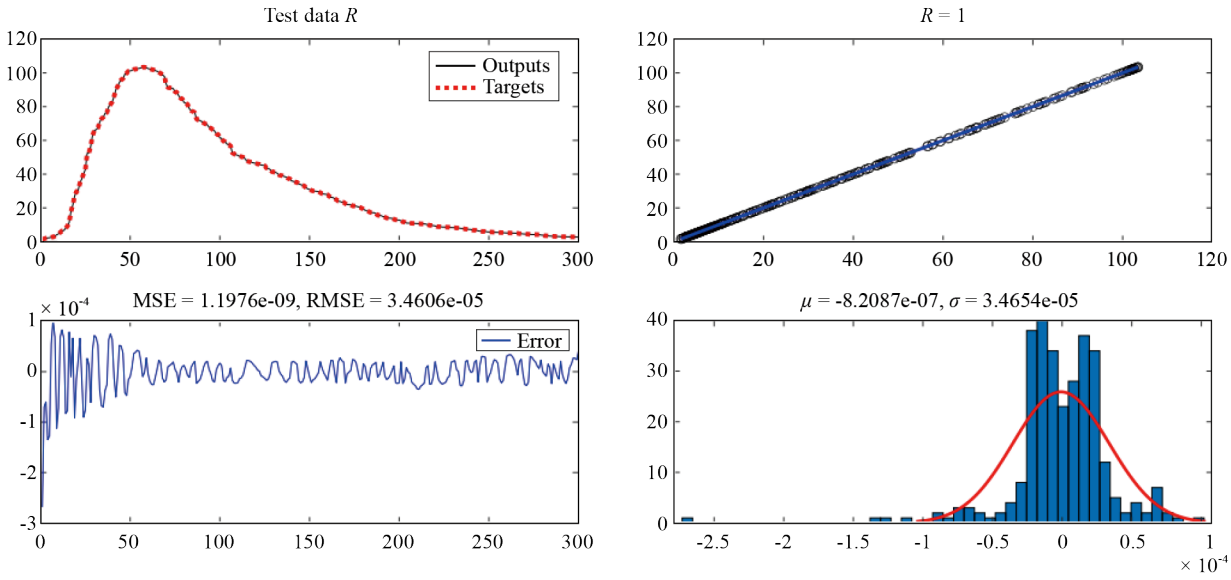


**Figure 32.** Graphical illustration of test data

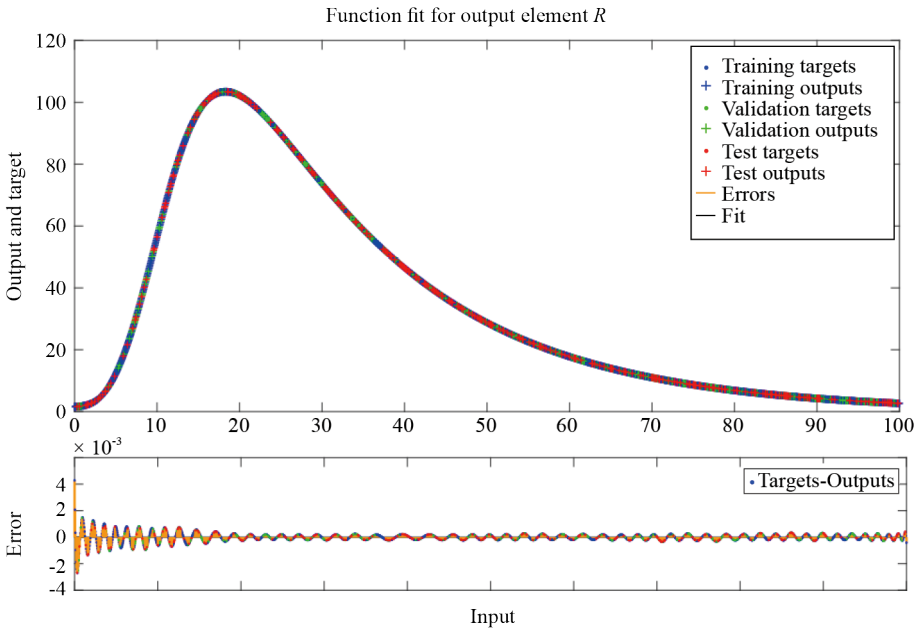


**Figure 33.** Graphical illustration of best function fit for data of $R$

In Figures 11-16, Figures 17-22, Figures 23-28, and Figures 29-34, where we have presented the simulations of all data, train data, validation data, test data, best function fit corresponding to each class of the considered model and performance analysis. The total number of epoches was 1,000, where the stopped values were 797 and 555 for $S$ and $V$ respectively in computational analysis. The initial values to achieve the target value 1,000 for susceptible and vaccinated classes for performance analysis were 36.4 and 23.5 respectively, while stopping values were 8.02e-10 and 2.19e-10. The gradient value for both $S$ and $V$ classes was computed at initial stage 99 and 95 and stopping values were 9.23e-08 and 8.06e-07 respectively. The target values during gradient computation was for both mentioned classes recorded as 1e-07. The value of $\mu$ for both mentioned classes as recorded as 0.001 initial, stopping 1e-11 and 1e-10 respectively, the target

was 1e + 10 for both $S$ and $V$. In the same way the echoes were recorded at stopping stage for $I$ and $R$ are 94 and 503 respectively. The performance analysis for $I$ and $R$ was recorded initial 87.3 and 30 while stoping values were 1.94e-09 and 4.51e-13. The gradient values for infected and recovered class were recorded as 214 and 78.1 initial and 3.23e-05 and 5.05e-08 at stopping position, while the target value was computed as 1e-07 for both classes. The value of $\mu$ for both mentioned classes was 0.001 at initial stage, while at stopping stage 1e-11 and 1e-12 respectively corresponding to target value 1e + 10 for both $I$ and $R$ respectively. In addition, the RMSE and MSE together with regression coefficient which is 1 have been presented for all classes in Figures 11-16, Figures 17-22, Figures 23-28, and Figures 29-34 respectively. Here, we remark that we have compared the numerical results of all classes with the predicted values due to ANNs in Figure 35. We see that the maximum absolute error is bellow $1 \times 10^{-2}$. This amount shows that the numerical values have close agreement with the predicted values.

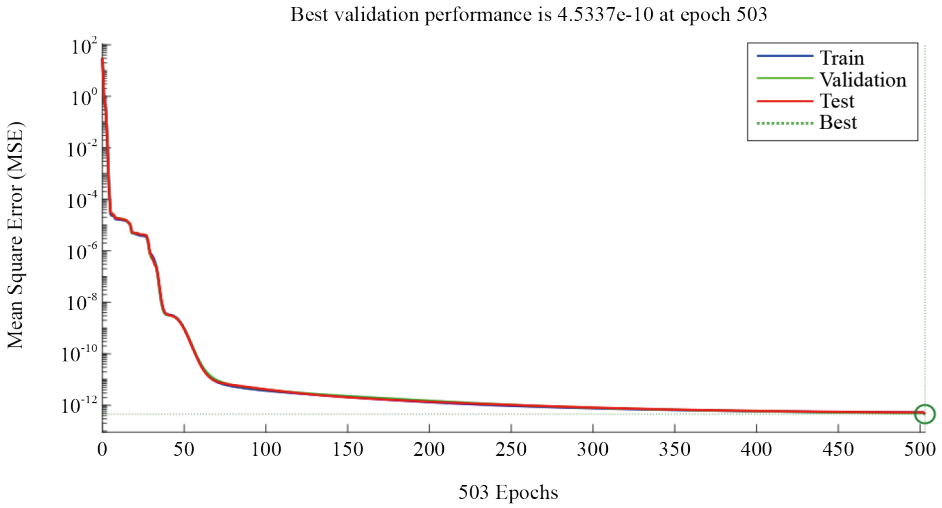


**Figure 34.** Graphical illustration of performance analysis using ANNs

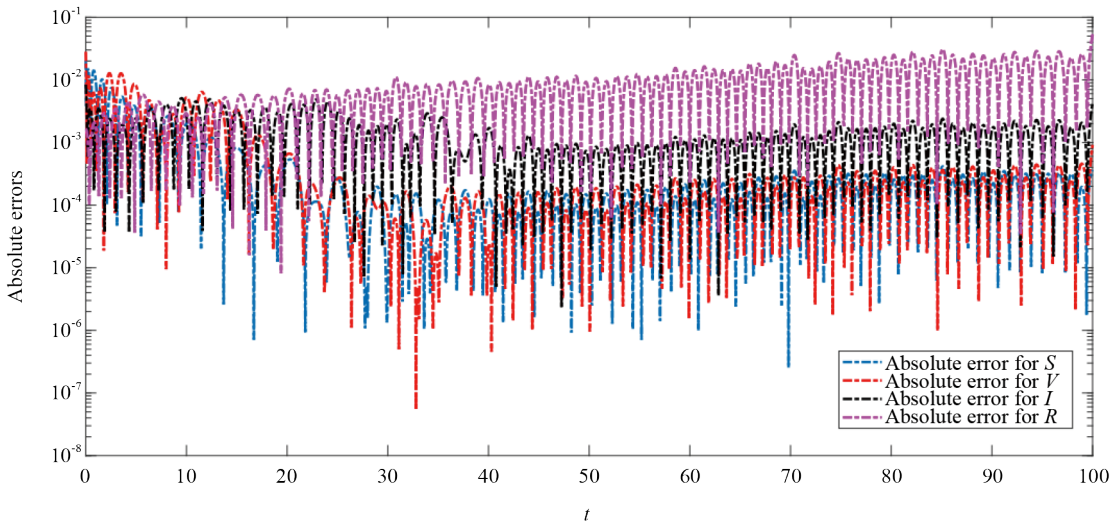


**Figure 35.** Absolute errors for all four compartment of model between numerical and predicted values

Offer superior performance in handling large-scale, complex, and unstructured data, such as images, audio, and text.

## 7. Conclusion

In recent time, the use of AI based NNs plays a significant role in computational analysis for the future prediction. These NNs offer superior performance to handle large scale complex and unstructured data like in images, audio or text. Their main benefits over conventional machine learning include scalability, enhanced accuracy, large model capacity for complicated pattern recognition, and automatic feature extraction which does away with manual engineering. Therefore motivated by the mentioned use, a discrete type mathematical model of four compartments was analyzed by using the Caputo difference operator with fractional order. Existence and uniqueness corresponding to solution of the mentioned model was investigated. Sufficient conditions were deduced under which the considered model has a unique solution. The result related to U-H stability was also given. Disease free equilibrium point was calculated. The expression for basic reproductive number was derived. Sensitivity analysis has been studied by using direct method and the sensitivity of parameters was analyzed. Numerical results against different fractional orders were presented graphically for all compartments. Finally a detailed analysis based on artificial deep neural networks has been presented. Several results regarding training data, validation, test and all data were investigated. Regression coefficient and absolute errors for all compartments were demonstrated graphically. From the graphical illustration, we concluded that the numerical data have close agreement with predicted outcomes. Hence, ANNs can be utilized as powerful tools in epidemiological models to investigate and predicted the future outcomes. Since the uncertainty in the availability of real data, yet it is not possible to construct perfect artificial neural network with 100% efficiency.


## Acknowledgment

Authors are thankful to Prince Sultan University for paying the APC and support.

## Funding source

This research is supported by Prince Sultan University for APC.


## Conflict of interest

The authors declare no competing financial interest.

## References


[1] Siettos CI, Russo L. Mathematical modeling of infectious disease dynamics. *Virulence*. 2013; 4(4): 295-306. Available from: https://doi.org/10.4161/viru.24041.

[2] Huppert A, Katriel G. Mathematical modelling and prediction in infectious disease epidemiology. *Clinical Microbiology and Infection*. 2013; 19(11): 999-1005. Available from: https://doi.org/10.1111/1469-0691.12308.

[3] Gómez S, Arenas A, Borge-Holthoefer J, Meloni S, Moreno Y. Discrete-time Markov chain approach to contact-based disease spreading in complex networks. *Europhysics Letters*. 2010; 89(3): 38009. Available from: https://doi.org/10.1209/0295-5075/89/38009.

[4] Sitthiwirattham T, Zeb A, Chasreechai S, Eskandari Z, Tilioua M, Djilali S. Analysis of a discrete mathematical COVID-19 model. *Results in Physics*. 2021; 28: 104668. Available from: https://doi.org/10.1016/j.rinp.2021.104668.

[5] Nabil H, Tayeb H. The impact of the Caputo fractional difference operator on the dynamical behavior of a discrete-time SIR model for influenza A virus. *Physica Scripta*. 2024; 99(11): 115269. Available from: https://doi.org/10.1088/1402-4896/ad8703.

[6] Coll C, Herrero A, Ginestar D, Sánchez E. The discrete fractional order difference applied to an epidemic model with indirect transmission. *Applied Mathematical Modelling*. 2022; 103: 636-648. Available from: https://doi.org/10.1016/j.apm.2021.11.002.

[7] Dhakshinamoorthy V, Wu GC, Banerjee S. *Chaotic Dynamics of Fractional Discrete Time Systems*. New York: CRC Press; 2024. Available from: https://doi.org/10.1201/9781003425113.

[8] Djenina N, Ouannas A, Batiha IM, Grassi G, Oussaeif TE, Momani S. A novel fractional-order discrete SIR model for predicting COVID-19 behavior. *Mathematics*. 2022; 10(13): 2224. Available from: https://doi.org/10.3390/math10132224.

[9] Coll C, Ginestar D, Herrero A, Sánchez E. Effectivity of the vaccination strategy for a fractional-order discrete-time SIC epidemic model. *Mathematical Modelling and Analysis*. 2024; 29(3): 525-545. Available from: https://doi.org/10.3846/mma.2024.19354.

[10] GümüÀŸ ÂZ, Selvam AG, Vianny DA. Bifurcation and stability analysis of a discrete time SIR epidemic model with vaccination. *International Journal of Analysis and Applications*. 2019; 17(5): 809-820.

[11] Dong S, Xu L, Yana A, Lan ZZ, Xiao D, Gao B. Application of a time-delay SIR model with vaccination in COVID-19 prediction and its optimal control strategy. *Nonlinear Dynamics*. 2023; 111(11): 10677-10692. Available from: https://doi.org/10.1007/s11071-023-08308-x.

[12] Marinov TT, Marinova RS. Adaptive SIR model with vaccination: Simultaneous identification of rates and functions illustrated with COVID-19. *Scientific Reports*. 2022; 12(1): 15688. Available from: https://doi.org/10.1038/s41598-022-20276-7.

[13] Gokbulut N, Amilo D, Kaymakamzade B. Fractional SVIR model for COVID-19 under Caputo derivative. *Journal of Biometry Studies*. 2021; 1(2): 58-64. Available from: https://doi.org/10.29329/JofBS.2021.349.04.

[14] de Miguel-Arribas A, Aleta A, Moreno Y. Impact of vaccine hesitancy on secondary COVID-19 outbreaks in the US: An age-structured SIR model. *BMC Infectious Diseases*. 2022; 22(1): 511. Available from: https://doi.org/10.1186/s12879-022-07486-0.

[15] Khan H, Alzabut J, Tunç O, Kaabar MK. A fractal-fractional COVID-19 model with a negative impact of quarantine on the diabetic patients. *Results in Control and Optimization*. 2023; 10: 100199. Available from: https://doi.org/10.1016/j.rico.2023.100199.

[16] Alkhazzan A, Wang J, Nie Y, Khan H, Alzabut J. A novel SVIR epidemic model with jumps for understanding the dynamics of the spread of dual diseases. *Chaos*. 2024; 34(9): 093119. Available from: https://doi.org/10.1063/5.0175352.

[17] Podlubny I. *Fractional Differential Equations: An Introduction to Fractional Derivatives, Fractional Differential Equations, to Methods of Their Solution and Some of Their Applications*. Amsterdam: Elsevier; 1999.

[18] Goodrich C, Peterson AC. *Discrete Fractional Calculus*. Cham: Springer; 2015. p.978-983. Available from: https://doi.org/10.1007/978-3-319-25562-0.

[19] Wu GC, Wu ZQ, Ji L. Machine learning to discover discrete fractional chaotic models. *Journal of Computational and Applied Mathematics*. 2026; 473: 116869. Available from: https://doi.org/10.1016/j.cam.2025.116869.

[20] Wu GC, Baleanu D. Discrete fractional logistic map and its chaos. *Nonlinear Dynamics*. 2014; 75: 283-287. Available from: https://doi.org/10.1007/s11071-013-1065-7.

[21] Khennaoui AA, Ouannas A, Bendoukha S, Grassi G, Wang X, Pham VT, et al. Chaos, control, and synchronization in some fractional-order difference equations. *Advances in Difference Equations*. 2019; 2019(1): 412. Available from: https://doi.org/10.1186/s13662-019-2343-6.

[22] Rajagopal K, Hasanzadeh N, Parastesh F, Hamarash II, Jafari S, Hussain I. A fractional-order model for the novel coronavirus (COVID-19) outbreak. *Nonlinear Dynamics*. 2020; 101(1): 711-718. Available from: https://doi.org/10.1007/s11071-020-05757-6.

[23] Khan H, Aslam M, Rajpar AH, Chu YM, Etemad S, Rezapour S, et al. A new fractal-fractional hybrid model for studying climate change on coastal ecosystems from the mathematical point of view. *Fractals*. 2024; 32(2): 2440015. Available from: https://doi.org/10.1142/S0218348X24400152.

[24] Djeddi K, Bouali T, Msmali AH, Ahmadini AA, Koam AN. Study models of COVID-19 in discrete-time and fractional-order. *Fractal and Fractional*. 2023; 7(6): 446. Available from: https://doi.org/10.3390/fractalfract7060446.

[25] Agatonovic-Kustrin S, Beresford R. Basic concepts of artificial neural network (ANN) modeling and its application in pharmaceutical research. *Journal of Pharmaceutical and Biomedical Analysis*. 2000; 22(5): 717-727. Available from: https://doi.org/10.1016/S0731-7085(99)00272-1.

[26] Ghaboussi J, Pecknold DA, Zhang M, Haj-Ali RM. Autoprogressive training of neural network constitutive models. *International Journal for Numerical Methods in Engineering*. 1998; 42(1): 105-126. Available from: https://doi.org/10.1002/(SICI)1097-0207(19980515)42:1<105::AID-NME356>3.0.CO;2-V.

[27] Shafiq A, Çolak AB, Sindhu TN, Lone SA, Alsubie A, Jarad F. Comparative study of artificial neural network versus parametric method in COVID-19 data analysis. *Results in Physics*. 2022; 38: 105613. Available from: https://doi.org/10.1016/j.rinp.2022.105613.

[28] Ning X, Jia L, Wei Y, Li XA, Chen F. Epi-DNNs: Epidemiological priors informed deep neural networks for modeling COVID-19 dynamics. *Computers in Biology and Medicine*. 2023; 158: 106693. Available from: https://doi.org/10.1016/j.compbiomed.2023.106693.

[29] Abdeljawad T, Shah K, Bushnaq S, Pongsopa J, Sitthiwirattham T. Using machine learning techniques to investigate a discreet type mathematical model of psychological mental disease. *Alexandria Engineering Journal*. 2025; 133: 157-171. Available from: https://doi.org/10.1016/j.aej.2025.11.017.

[30] Qasim M, Ali H, Farooq A, Kamran M, Ahmad H, Awwad FA, et al. Intelligent neural framework for modeling the lifestyle-induced remission in the type 2 diabetes. *Chaos, Solitons & Fractals*. 2026; 205: 117841. Available from: https://doi.org/10.1016/j.chaos.2025.117841.

[31] Shah K, Liu W, El Yamani MA, Khan U, Rehman S, Farooq A. Neural network approach for cholera dynamics: Integrating deterministic and stochastic insights. *Knowledge-Based Systems*. 2024; 296: 111957. Available from: https://doi.org/10.1016/j.knosys.2024.111957.

[32] Qadeer Khan A, Tasneem M, Younis BA, Ibrahim TF. Dynamical analysis of a discrete-time COVID-19 epidemic model. *Mathematical Methods in the Applied Sciences*. 2023; 46(4): 4789-4814. Available from: https://doi.org/10.1002/mma.8806.

[33] Li MT, Cui J, Zhang J, Sun GQ. Transmission analysis of COVID-19 with discrete time imported cases: Tianjin and Chongqing as cases. *Infectious Disease Modelling*. 2021; 6: 618-631. Available from: https://doi.org/10.1016/j.idm.2021.03.007.

[34] Tu JV. Advantages and disadvantages of using artificial neural networks versus logistic regression for predicting medical outcomes. *Journal of Clinical Epidemiology*. 1996; 49(11): 1225-1231. Available from: https://doi.org/10.1016/S0895-4356(96)00002-9.

[35] Abbes A, Ouannas A, Shawagfeh N, Jahanshahi H. The fractional-order discrete COVID-19 pandemic model: stability and chaos. *Nonlinear Dynamics*. 2023; 111(1): 965-983. Available from: https://doi.org/10.1007/s11071-022-07766-z.

[36] Sousa GA, Souza DL, Gabrick EC, dos Reis PD, Bentivoglio LE, Batista AM, et al. Continuous and discrete compartmental models for infectious disease. *Brazilian Journal of Physics*. 2025; 55(3): 137. Available from: https://doi.org/10.1007/s13538-025-01771-4.

[37] He ZY, Abbes A, Jahanshahi H, Alotaibi ND, Wang Y. Fractional-order discrete-time SIR epidemic model with vaccination: Chaos and complexity. *Mathematics*. 2022; 10(2): 165. Available from: https://doi.org/10.3390/math10020165.

[38] Li X, Jiang W. Solving fractional difference equations using the Laplace transform method. *Abstract and Applied Analysis*. 2014; 2014(1): 230850. Available from: https://doi.org/10.1155/2014/230850.

[39] Hoan LV, Akinlar MA, Inc M, Gómez-Aguilar JF, Chu YM, Almohsen B. A new fractional-order compartmental disease model. *Alexandria Engineering Journal*. 2020; 59(5): 3187-3196. Available from: https://doi.org/10.1016/j.aej.2020.07.040.

[40] Chen F, Zhou Y. Existence and Ulam stability of solutions for discrete fractional boundary value problem. *Discrete Dynamics in Nature and Society*. 2013; 2013(1): 459161. Available from: https://doi.org/10.1155/2013/459161.

[41] Rus IA. Some variants of contraction principle, generalizations and applications. *Studia Universitatis Babes-Bolyai Mathematica*. 2016; 61(3): 343-358.

[42] Worldometer. *Pakistan COVID-coronavirus cases*. 2024. Available from: https://www.worldometers.info/ [Accessed 13rd April 2024].

[43] Imran M, Khan S, Khan S, Uddin A, Khan MS, Ambade P. COVID-19 situation in Pakistan: A broad overview. *Respirology*. 2021; 26(9): 891-892. Available from: https://doi.org/10.1111/resp.14093.

[44] Eiman, Shah K, Sarwar M, Abdeljawad T. On mathematical model of infectious disease by using fractals fractional analysis. *Discrete and Continuous Dynamical Systems-S*. 2024; 17(10): 3064-3085. Available from: https://doi.org/10.3934/dcdss.2024073.